Journal of Catalysis 438 (2024) 115705

Contents lists available at ScienceDirect

Journal of Catalysis

journal homepage: www.elsevier.com/locate/jcat

Research article

Sunlight induced C-H arylation of aromatic heterocycles: First example of A_3 and A_2B type corroles as photoredox catalysts

Ashmita Jain, Shekhar Kumar, Sanyam, Anirban Mondal, Iti Gupta *

Indian Institute of Technology Gandhinagar, Palaj, Gandhinagar, Gujarat 382355, India

ARTICLE INFO

Keywords:
Borylation
C–H arylation
Corrole
Crystal structure
Photo-redox reaction
Photo-catalysis

ABSTRACT

The visible light mediated metal-free approach has been developed for C–H arylation and borylation employing anilines as starting material. A series of *meso*-aryl corroles (A_3 and A_2B type) were synthesized and their catalytic potential was tested in blue light and sunlight. The method includes substituted anilines as source of expensive aryl diazonium salts and utilizes only 0.5 to 1 mol% of corrole catalyst at room temperature. Corrole catalyst worked efficiently under the blue light/sunlight to produce heterobiaryls and aryl boronic esters in decent to good yields (15–80 %). Mechanistic insight was obtained from TD-DFT studies, which suggested single electron transfer (SET) from the singlet state of corrole catalyst to the aryl diazonium salt. The paper demonstrates corrole based photo-redox catalysis as a mild, green and eco-sustainable alternative for the C–H arylation reactions.

1. Introduction

Visible light being an abundant and sustainable source of energy can be used to accelerate organic transformations of molecules via photocatalyst [1]. Photochemical reactions offer the advantage of mild conditions over thermal reactions with high temperature, where light is used as a renewable and sustainable source of energy [2]. Under light irradiation, the photocatalyst in its excited state can exhibit photocatalysis by transferring energy to surrounding molecules such as molecular oxygen, heterocycle and other relevant molecules [3]. Apt photocatalyst that exhibits absorption in the visible region of spectra and matches the electrochemical and spectral requirement of the system is chosen [4]. Visible light offers to avert the product decomposition and side reactions as it can be absorbed by sensitizers but not by most organic compounds [5].

Since 1969, porphyrins have been employed as an effective photocatalyst for epoxidation, sulfoxidation, hydroxylation, carbonylation, C–H functionalization and arylation [6–9]. However, corroles found their applications in the field of photocatalysis much later around 2004. Corroles are best described as tetrapyrrolic macrocycles with three methine bridges and one direct pyrrole-pyrrole bond. They are analogous to porphyrins with inimitable photophysical and electrochemical properties [10]. Generally, corroles are more emissive than porphyrins; and their complexes with P, Al and Ga have higher fluorescent quantum yields (20–76 %) than the parent corrole. The chelation of corroles with heavy metals (Sb, Sn, Re, Au) can leads to substantial phosphorescent emission from triplet states at room temperature, enabling them as triplet photosensitizers for singlet oxygen generation and light assisted organic reactions. The molar absorption coefficients of corroles are much higher than the Ru- and Ir-polypyridyl complexes in the range of 400–500 nm. Also, triplet state lifetime of 5d metal complexes of corrole were found to be in the order of 56–80 micro seconds, much higher than the Ru- and Ir-polypyridyl complexes. Corroles may act as both photooxidant or photoreductant because their redox properties can be fine-tuned by halogens substitution at the corrole skeleton or changing the axial ligand attached to the central metal ion in the complex. These distinct features of corroles prompted the researchers to explore their photocatalytic potential for organic transformations. Gross and co-workers reported a handful of examples, including bromination, aziridination, and C–H activation [11,12]. Schoefberger and the group also employed bismuth corrole for sulfoxidation. Nocera and group used antimony oxo corroles with two quasi-reversible oxidations at + 0.57 V and + 0.76 V *vs.* Fc^+ /Fc for C–H activations [13] and results were compared with respective porphyrins [14].

Nonetheless, several examples of organic transformations by corrole are reported. First example of catalysis by corrole was reported by Gross and co-workers in 1999 [15]. They used iron corrole to catalyze the epoxidation, cyclopropanation and hydroxylation of alkene and found them to be almost as potent as corresponding porphyrins. After that, corroles were widely explored in catalysis, some of which includes

* Corresponding author.
E-mail address: iti@iitgn.ac.in (I. Gupta).

https://doi.org/10.1016/j.jcat.2024.115705
Received 26 February 2024; Received in revised form 5 August 2024; Accepted 9 August 2024
Available online 13 August 2024

sulfoxidation, hydroperoxidation, reduction of CO_2, activation of O_2 and group transfer catalysis such as cyclopropanation, C–H insertion of carbene, N–H insertion of carbene, aziridination, etc [16,17].

Photoredox catalysis found applications in water splitting, proton coupled electron transfer, CO_2 reduction, photovoltaics and the development of photo-electrochemical solar cells [18–21]. Apart from the above-stated applications, photoredox catalysis has come to the forefront as a powerful tool to execute the formation of challenging carbon–carbon and carbon-heteroatom bonds [22–24]. Traditional photoredox catalysts include organic dyes such as eosin Y and heavy metal complexes such as Ir and Ru complexes [25,26]. Limitations of organic dyes being pH sensitive and heavy metal complexes being expensive and toxic, motivated researchers to explore porphyrin as photocatalyst [27,28]. Organic dye eosin Y was employed by Konig and co-workers to photocatalyse C–H bond arylation of heteroarene with aryl diazonium salt [29]. Later, Gryko and co-workers used porphyrin to carry out this Meerwein's arylation [30]. The Pt(II) and Pd(II) complexes of tetra-aryl porphyrins have been employed as photocatalysts for the oxidation of organic substrates over the last few years [31–33]. Also, Meerwein's arylation of organic substrates was efficiently photocatalysed by Zn(II)porphyrins in the presence of visible light [34,35].

The chemistry of C–H activation reactions employing porphyrins and their metal complexes as photoredox catalysts is in early stages; and to the best of our knowledge there are no reports on photoredox catalysis utilizing corroles. In this work, we present the synthesis and characterization of *meso*-substituted corroles (A_3 and A_2B type). The visible light and sun-light assisted C–H arylation and borylation by photoredox mechanism was demonstrated by corroles. Corroles worked efficiently as photoredox catalysts for a variety of aromatic substrates and the reaction mechanism was investigated by DFT calculations.

2. Results and discussion

2.1. Synthesis

Corrole **C1** was synthesized by trifluoroacetic acid (TFA) catalysed condensation of pyrrole and 2,3,4,5,6-pentafluorobenzaldehyde using DCM as a solvent. Reaction involved the formation of bilane as an intermediate and was followed by treatment with *p*-chloranil as an oxidizing agent. Progress of the reaction was monitored by TLC which showed fluorescent spot corresponding to the corrole. In order to make *trans*-A_2B types corroles **C2** and **C3**, the [2 + 1] condensation of dipyrromethanes and aryl aldehydes was carried out. The key precursors, 5-pentafluorophenyl dipyrromethane and 5-(4-cyanophenyl) dipyrromethane were synthesized as per the mechanism reported in the literature [36]. One pot condensation of 5-pentafluorophenyl dipyrromethane with *p*-cyanobenzaldehyde in presence of TFA, followed by addition of *p*-chloranil yielded corrole **C2**. Similarly, corrole **C3** was synthesized by taking 5-(4-cyanophenyl) dipyrromethane and 2,3,4,5,6-pentafluorobenzaldehyde as reactant. Purification of corrole **C1, C2** and **C3** was performed in silica gel column chromatography and pure corroles were obtained in 6–15 % yield (Scheme 1). Synthesized compounds were characterized and given in SI. (Figure S1-S4).

2.2. X-ray Crystal structures

Corrole **C3** was crystallized as purple colour crystal in the mixture of tetrahydrofuran (THF) and pentane solution by diffusion method. The

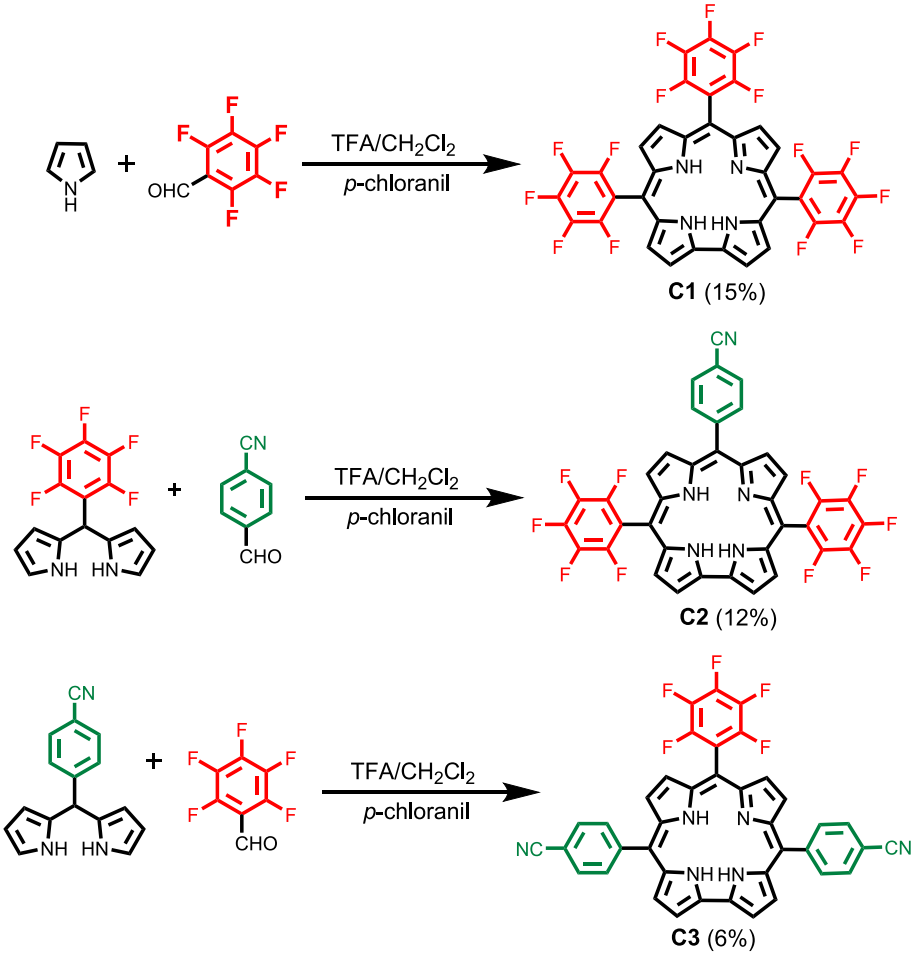

Scheme 1. Synthesis of free base corroles.

solid-state packing diagram of corrole **C3** (CCDC 2300649) depicted the presence of four molecules of free base corrole in a unit cell; and inner NH proton is H-bonded with the solvent in the solid state. In crystal structure of corrole, pyrrole rings exhibit deviation from planarity by turning either up or down from the mean plane (Fig. 1).

This puckered conformation is achieved to minimize the steric strain due to inner NH protons. The dihedral angle between corrole mean plane and *meso*-substituent [C4-C5-C27-C32, C16-C15-C20-C21 and C11-C10-C34-C39] were found to be 41.2(2)°, 52.7(2)° and 77.5(2)° respectively. The reported dihedral angles between *meso*-phenyl group (at C5, C10 and C15-positions) were 41.3°, 47.7°, and 46.3° for the H_3TPC (5,10,15-triphenyl) corrole [37,38].

2.3. Absorption and emission studies

The UV–visible absorption and fluorescence studies of corroles **C1-C3** were carried out in toluene and the data are compiled in Table 2.

Table 1
Crystal parameters of corrole **C3**.

Crystal parameters	
Empirical formula	$C_{39}H_{19}F_5N_6$
Formula weight	666.1591
Crystal colour, habit	Purple, plate
Crystal dimensions	0.562 × 0.174 × 0.056 mm
Crystal systemLattice parameters	Monoclinic a = 14.372(5) Å, b = 15.792(4) Å, c = 16.812 (4) Å, α = 90°, β = 112.199(8)°, γ = 90°, V=3532.9(17) Å^3
Lattice type, space group	P 1 21/c 1
Z value	2
R_1	0.0561
wR_2	0.2013
GOF	1.385

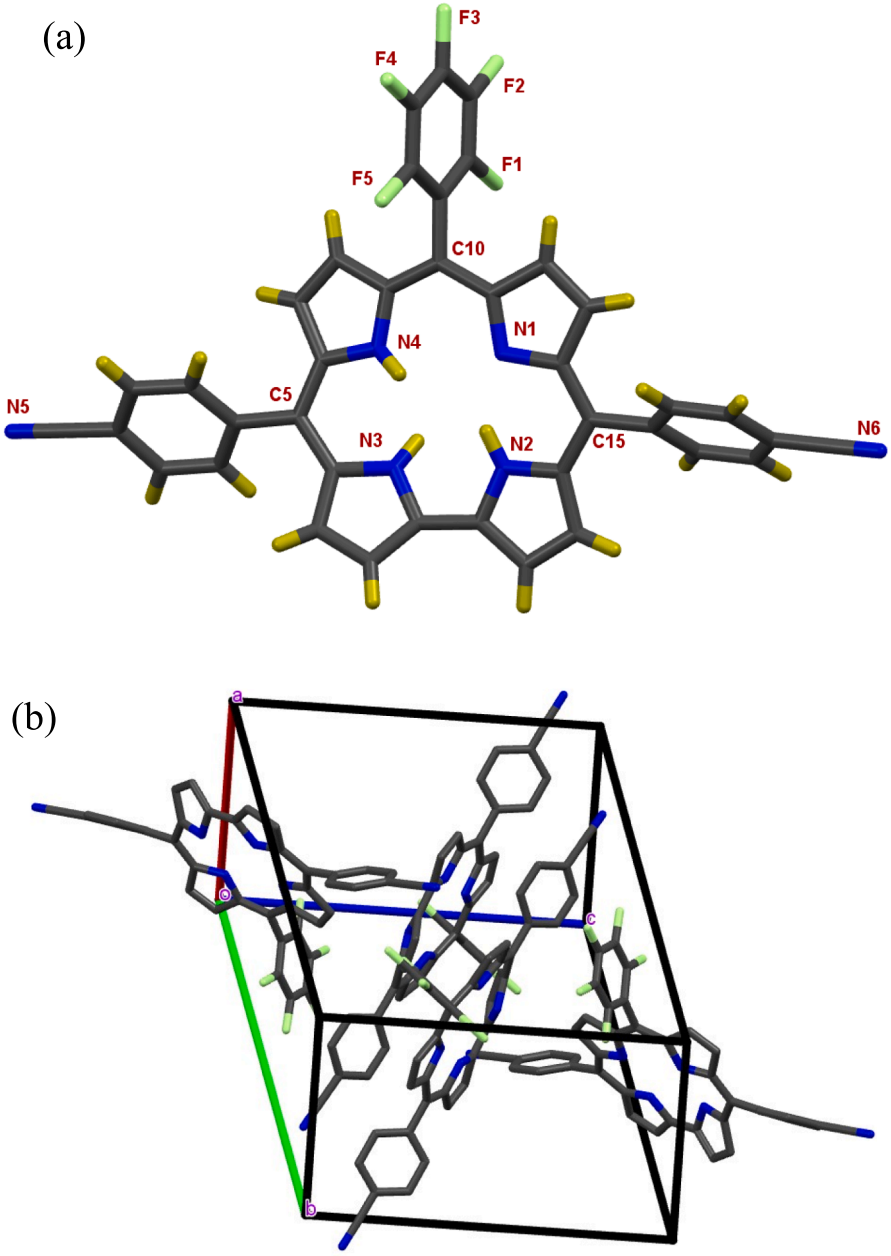

Fig. 1. (a) X-ray crystal structure of **C3**. (b) Packing diagram of **C3** in the unit cell (hydrogen atoms and solvent molecules are omitted for clarity).

Table 2
Photophysical data of corroles recorded in toluene. (λ_{ex} = 550 nm).

Corrole	λ_{abs} (nm) (log ε) in toluene	λ_{em} (nm)	Φ_f	Stokes shift (cm^{-1})	τ (ns)[a]
C1	415 (4.90), 568 (4.24), 606 (4.10)	647, 706 (sh)	0.14	992	4.4 ns
C2	420 (4.75), 567 (3.96), 613 (3.74)	659	0.21	1139	4.1 ns
C3	426 (4.74), 585 (4.03)	667	0.14	899	3.9 ns

a: excitation wavelength = 390 nm.

Fig. 2 shows the comparative absorption and emission spectra of the corroles. Absorption spectra of corrole follow the "Gouterman four orbital model", just like porphyrin [39]. Soret bands were slightly blue-shifted compared to analogous porphyrin due to the reduced symmetry of the ring [40]. The presence of three fully fluorinated benzene groups at *meso* position in **C1** corrole, makes it exhibit more hypsochromic shift as compared to corrole **C2** and **C3**, in consistent with previous studies [41]. High Stokes shift and fluorescence quantum yield were obtained as compared to analogous porphyrins [42,43]. Major fluorescence band for corrole **C1** was obtained at 647 nm along with a shoulder band at 706 nm. While for corroles **C2** and **C3**, only one fluorescence band was obtained at 659 and 667 nm, respectively. A bathochromic shift is observed in the emission spectra as the number of *p*-cyanophenyl group increases at *meso*-position. H_2TPP (Φ_f = 0.11) dissolved in toluene was taken as a standard and the fluorescence quantum yield of corrole **C1** to **C3** were determined by comparing their emission and absorption spectra with that of reference H_2TPP. For free base corroles **C1-C3,** the calculated fluorescence quantum yields were between 14 to 21 % (Table 2), considerably higher than the free base porphyrin (H_2TPP). The singlet state fluorescence lifetime (τ) of the corroles was recorded in DMSO; the decay profiles are shown in Figure S95. The observed singlet state lifetimes of corroles were around 3.9–4.4 ns (Table 2); suggesting that *meso*-aryl substituents have negligible influence on the corrole life time.

2.4. Electrochemical study

The cyclic voltammetry studies of corroles were carried out in dry dichloromethane with 0.1 M tetrabutylammonium perchlorate (TBAP) as a supporting electrolyte. Redox potential and reduction wave data are provided in Table 3 and Fig. 3, respectively. The free base corroles can show two–three oxidation and reduction processes in solvents like benzonitrile and pyridine [44]. Two oxidation waves were observed for the free base corroles **C1-C3** between 0.84 to 1.38 V, as shown in Table 3. The free base corroles **C1-C3** exhibited one electron reduction around −1.64 V in dry DCM (Table 3). However, in benzonitrile, only one oxidation wave was observed for the A_3 type corroles (*meso*-tri-pentafluorophenyl corrole and *meso*-tri-*p*-cyanophenyl) at 0.31 and 0.11 V, respectively [44]. On the other hand, the reduction potential values were very similar to the reported A_3 type parent molecules (−1.55 V). As the number of pentafluorophenyl groups are decreasing from **C1** to **C3**, a cathodic shift in the oxidation potentials was observed (Table 3), facilitating the ease in oxidation of **C2** and **C3**. Employing the redox potential data and emission maxima of corroles, the zero-zero excited energy ($E_{0,0}$) and the excited state oxidation potentials (E_{ox}*) of **C1** to **C3** were calculated (Table 3, Table S1) by using the reported method [30].

3. Photoredox catalysis

3.1. Hetero-Arylation reactions

Visible light is an environmentally friendly and inexpensive source of energy that can be utilized for chemical transformations in a sustainable way. Hetero-biaryls are important part of pharmaceutical compounds, natural products and organic functional materials [45–47]. Light assisted C–H arylation reactions are good alternative to the transition metal catalysed cross coupling reactions. To standardize the reaction conditions, parameters like solvent, catalysts and light wavelength were varied for a representative reaction between furan and 4-nitroaniline (Table 4). Slight increase in yield was obtained in the case of corrole catalyst **C2** in dimethylsulfoxide (DMSO) with blue light irradiation (entry 2). The other two corrole catalysts **C1** and **C3** gave slightly lower yields under same conditions (entries 1 and 3, respectively). The catalyst amount suitable for this reaction was found to be 0.5 mol % and the higher amounts of the corrole **C2** were not effective (entries 13 and 14). Other polar solvents, such as dimethylformamide (DMF), dichloromethane (DCM), chloroform ($CHCl_3$), acetonitrile (MeCN), and their combinations were found to be less effective (entries 4–11). Significantly lower yield was obtained when white light was used to irradiate the **C2** catalyst under same conditions (entry 12).

In the control experiments, a considerably lower amount of product was found when the reaction was carried out without a catalyst or light (entries 15 and 16, respectively). When thiophene and *N*-Boc pyrrole were used with nitroaniline in the absence of catalyst or light, trace amount of product was observed on TLC.

Table 3
Cyclic Voltammetry data of compounds in dry DCM with TBAP as supporting electrolyte, at scan rate 50 mVs^{-1}.

Corrole	$E_{1/2}$(ox) *vs* SCE (V)		$E_{1/2}$(red) *vs* SCE (V)	E_{ox}* [Cor^+/Cor*] (V)	$E_{0,0}$ (V)
	I	II	I		
C1	1.22	1.38	−1.64	−0.72	1.94
C2	0.95	1.18	−1.66	−0.93	1.88
C3	0.94	1.04	−1.61	−0.91	1.85

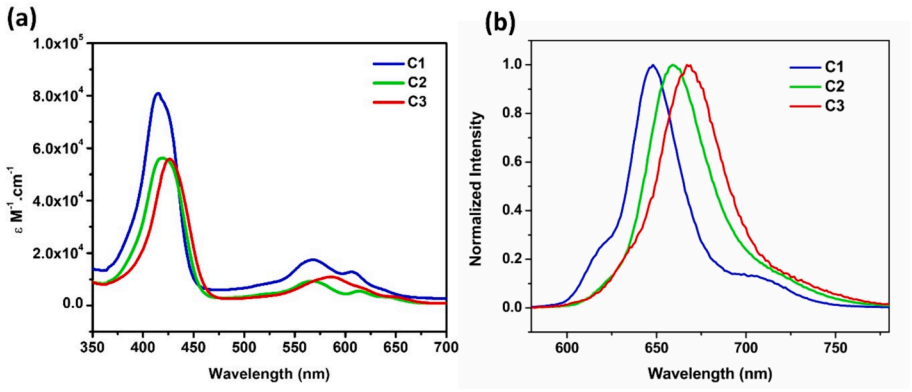

Fig. 2. (a) Comparison of UV–visible absorption spectra, and (b) Fluorescence spectra of corroles (λ_{ex} = 550 nm) recorded in toluene.

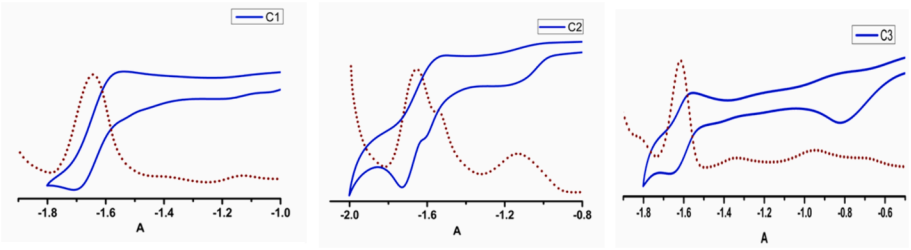

Fig. 3. Cyclic Voltammogram of corroles showing comparison of reduction waves (solid lines) and differential pulse voltammograms (dashed lines). (a) **C1**; (b) **C2** and (c) **C3** in dry DCM with 0.1 M TBAP as supporting electrolyte at scan rate 50 mV/sec.

Table 4
Optimization of reaction conditions for arylation of furan.[a]

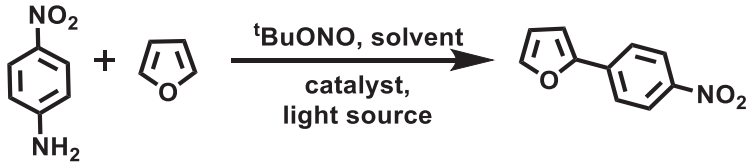

Entry	Catalyst	Solvent	Light source	Catalyst loading (mol%)	Yield[b] (%)
1	**C1**	DMSO	Blue	0.5	78
2	**C2**	DMSO	Blue	0.5	80
3	**C3**	DMSO	Blue	0.5	71
4	**C2**	DCM	Blue	0.5	78
5	**C2**	$CHCl_3$	Blue	0.5	41
6	**C2**	DMF	Blue	0.5	77
7	**C2**	MeCN	Blue	0.5	40
8	**C2**	DMSO+DMF	Blue	0.5	75
9	**C2**	DMSO+$CHCl_3$	Blue	0.5	66
10	**C2**	DMSO+MeOH	Blue	0.5	37
11	**C2**	DMSO+ACN	Blue	0.5	68
12	**C2**	DMSO	White	0.5	65
13	**C2**	DMSO	Blue	0.75	76
14	**C2**	DMSODMSODMSO	Blue	1	67
15[c]	–		Blue	−0.5	10
16[d]	**C2**		–		12

[a]Reaction conditions: 4- nitroaniline (0.30 mmol), furan (3.0 mmol), [t] BuONO (0.45 mmol) irradiation with light (24 W) for 30 min under N_2 atm at rt, [b] Isolated yields after purification, [c] without catalyst, [d] without light.

The reaction involves 4-nitroaniline, [t]BuONO and furan with corrole catalyst **C2** under blue LED for 30 mins in an inert atmosphere. Compared to eosin Y, which takes 2 h, the **C2** catalyst completes the reaction in just 30 min. Different substituted anilines were reacted with furan to provide the corresponding hetero-biaryls; the results are presented in Table 5.

Furthermore, the corrole catalyst **C2** worked efficiently when similar reactions were performed under sunlight for 30 min (Table 5). This clearly suggests that corrole **C2** is energy efficient and green catalyst for C–H arylation reactions. Furan and thiophene underwent arylation with *p*-nitro, *p*-cyano, *p*-acetyl and halogenated anilines; reaction displayed excellent functional group tolerance particularly with halogens and they remained intact after arylation. The arylation of furan and thiophene with 2-ethynylaniline derivatives went on smoothly to produce the corresponding (2-alkynylaryl) substituted heteroarenes (**2j- 2 l** and **3j- 3 l**) in good yields (Tables 5 and 6).

The (2-alkynylaryl) substituted heteroarenes are important precursors for the thiophene and furan containing medicinal compounds. C–H arylation of *N*-Boc pyrrole was also successfully demonstrated with **C2** catalyst in blue light with substituted anilines (Table 7). The reaction was compatible with *p*-nitro, *p*-cyano, *p*-acetyl and halogenated anilines and arylated *N*-Boc pyrroles were obtained in decent yields (32–56 %, Table 7). In general, arylation reactions gave higher amounts of products when furan, thiophene and *N*-Boc pyrrole were reacted with electron-deficient anilines. Also, the sunlight induced arylation of furan and thiophene afforded comparable or slightly less yields of the products with respect to the corresponding blue light sensitized reactions (Tables 5 and 6). C–H arylation of 4-Aminobenzonitrile with furan was scaled up by 10 times, and yield was 61 % (Scheme 2). As per the previous reports, the C–H arylation reactions of furan, thiophene and *N*-Boc pyrrole with aniline derivatives followed a radical mechanism [48]. Plausible mechanism is depicted in Fig. 4. It was supported by the **C2** catalysed reaction of *p*-nitroaniline with [t]BuONO under blue light exposure (Scheme 3). When radical scavenger 2,2,6,6-tetramethyl-1-piperidin-1-oxyl (TEMPO) was added to the reaction, the corresponding adduct was formed as noticed in the mass analysis and characterized via NMR. (Figure S59-S60).

3.2. Borylation reactions

The transition metal-catalyzed cross-coupling reactions are broadly employed in synthesising biaryls or hetero-biaryl compounds [49]. Arylboronic acids or arylboronic esters are essential to synthesize a variety of organic molecules and pharmaceutical compounds [50,51]. C–H borylation of aromatic compounds can be achieved by iridium and rhodium complexes utilizing boronic esters (B_2pin_2 /B_2Epin_2) [52–54]. The borylation of arylamine was demonstrated with visible light and sunlight irradiation of catalyst **C2**.

To optimize the solvent conditions, nitroaniline was reacted with [t]BuONO and B_2pin_2 under blue light for 1 h at room temperature

Table 5
Scope of arylation of furan with substituted anilines in blue light and sunlight.[a.]

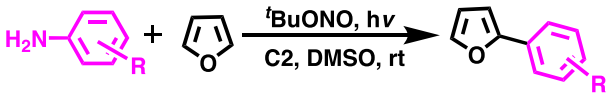

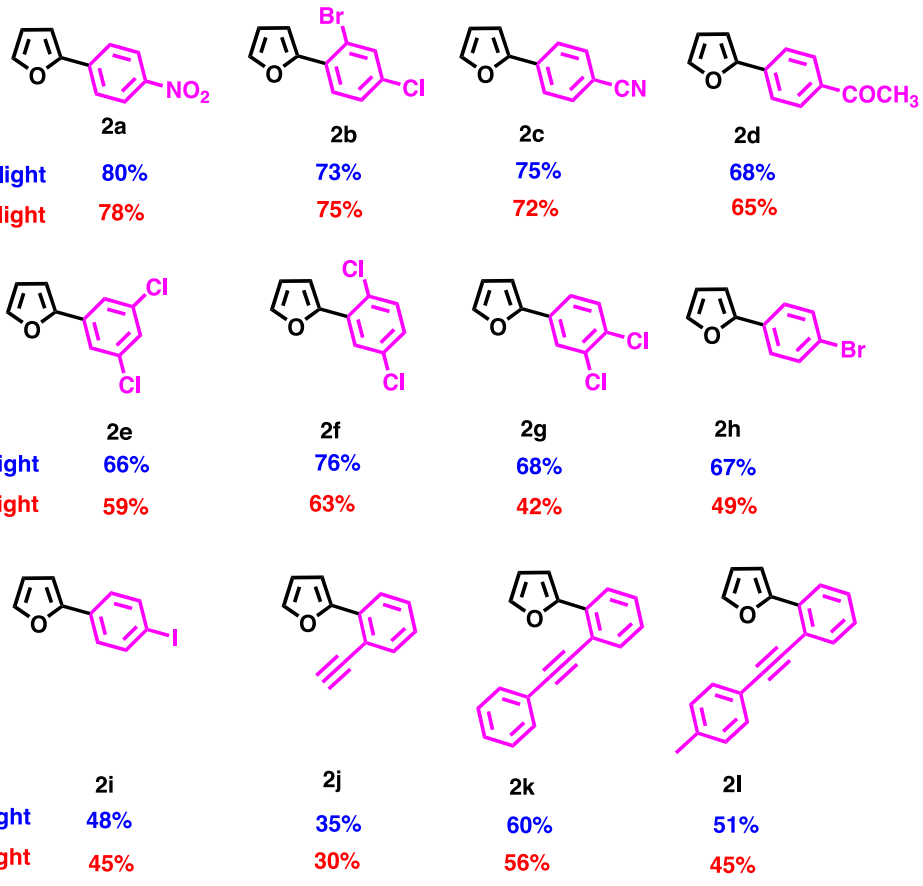

[a]Reaction conditions: Substituted anilines (0.30 mmol), furan (3.0 mmol), **C2** (0.5mol%), ^{t}BuONO (0.45 mmol) irradiation with light (blue light/sunlight) for 30 min under N_2 atm at rt.

(Table 8). In DMSO, DMF, toluene and chloroform the product yields were lower (32–51 %), whereas in nitromethane and DCM the yields increased to 60–61 %, respectively. Highest amount of borylation product was obtained in MeCN (entry 3, 71 %) with 1 mol% of corrole catalyst **C2**. Also, no product formation was observed when the reaction was carried out in the absence of light or catalyst. After optimizing the reaction conditions, the substrate scope was investigated for borylation reaction and findings are summarized in Table 9.

The *p*-nitro, *p*-cyano and *p*-halogenated anilines were subjected to borylation with ^{t}BuONO and B_2pin_2 under blue light (24 W) at room temperature. Similar to the C–H arylation reaction of furan and thiophene, the borylation reactions afforded higher yields when aniline with electron-withdrawing groups was treated with B_2pin_2 under the same conditions (Table 9, 5a-5c). Whereas, halogenated anilines underwent borylation reaction to afford the products in 30–63 % yields (Table 9, 5d-5f). Furthermore, 1 mol% of **C2** catalyst worked efficiently under sunlight for borylation reaction and substituted anilines afforded products in moderate to good yields (35–71 %).

Likewise, the substituted anilines afforded decent yields of borylated products when treated with B_2Epin_2 under similar conditions (Table 10). In general, electronic effect of the substituents on anilines was not prominent and low to moderate yields of borylated products (15–38 %) were obtained under blue light or sunlight exposure (Table 10). The examples clearly demonstrate that corrole **C2** is a promising catalyst for the C–H arylation and borylation of aromatic substrates.

3.3. Computational studies

All the quantum mechanical calculations were done with the help of the Gaussian program v.09, and Gauss view was used for visualization [55]. The ground state optimization of all three corrole systems was performed within density functional theory (DFT), using B3LYP functional and the basis set 6-311G(d,p). To add the solvent effect, a conductor polarizable continuum model was used with the solvent dimethyl sulfoxide ($\varepsilon = 46.83$). Similarly, the excited state optimization was performed within the time-dependent-DFT (TD-DFT) framework at the same theory and solvent model level. Additionally, we optimized cation and anion for each corrole to calculate the redox potential values for the ground and excited states. The electron density difference between the excited and ground states was computed employing ORCA v5.02 [56] using the same functional and basis set mentioned above. The difference density plots were generated using multiwfn3 [57] and VESTA [58] programs.

The computed frontier molecular orbitals (FMOs), absorption maxima, and the corresponding oscillator strengths (*f*) are listed in Fig. 5 and Table 11. The optimized ground-state geometries of the corroles are

Table 6
Scope of arylation of thiophene with substituted anilines in blue light and sunlight.[a]

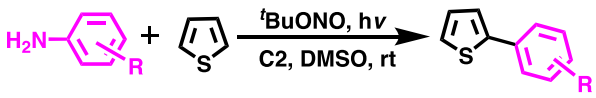

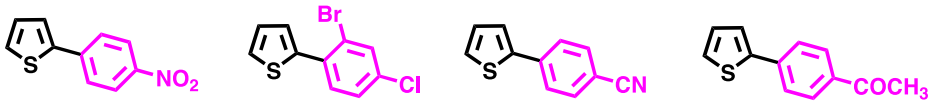

	3a	3b	3c	3d
Blue light	64%	63%	54%	38%
Sun light	57%	61%	49%	35%

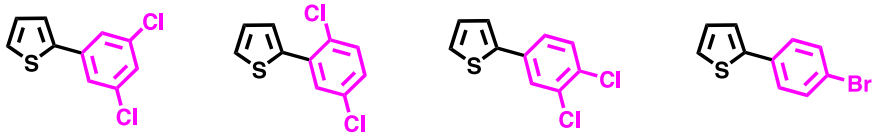

	3e	3f	3g	3h
Blue light	58%	53%	45%	35%
Sun light	55%	48%	42%	52%

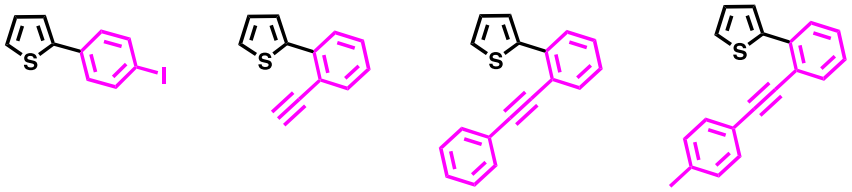

	3i	3j	3k	3l
Blue light	26%	21%	40%	33%
Sun light	33%	21%	34%	28%

[a] Reaction conditions: Substituted anilines (0.30 mmol), thiophene (3.0 mmol), **C2** (0.5 mol%), ^{t}BuONO (0.45 mmol), irradiation with light (blue light/sunlight) for 30 min under N_2 atm at rt.

Table 7
Scope of arylation of *N*-Boc pyrrole with substituted anilines in blue light.[a.]

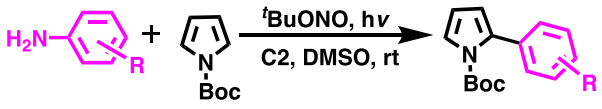

	4a	4b	4c	4d
Blue light	45%	56%	50%	32%

[a]Reaction conditions: Substituted anilines (0.30 mmol), *N*-Boc pyrrole (0.6 mmol), **C2** (0.5 mol%), ^{t} BuONO (0.45 mmol), irradiation with blue light (24 W) for 30 min under N_2 atm at rt.

shown in Fig. 6a and Figures S87-S88 of the SI. DFT cartesian co-ordinates of corrole and the intermediated are depicted in Table S2. For corroles, **C1** and **C3,** the HOMO-1 to LUMO+1 is the dominant transition. Whereas, for corrole **C2**, the significant transitions occurred from HOMO-1 to LUMO and HOMO to LUMO+1 orbitals. A decent agreement was seen between the estimated and experimentally

Scheme 2. Scale up of arylation of furan with 4-aminobenzonitrile in blue light.

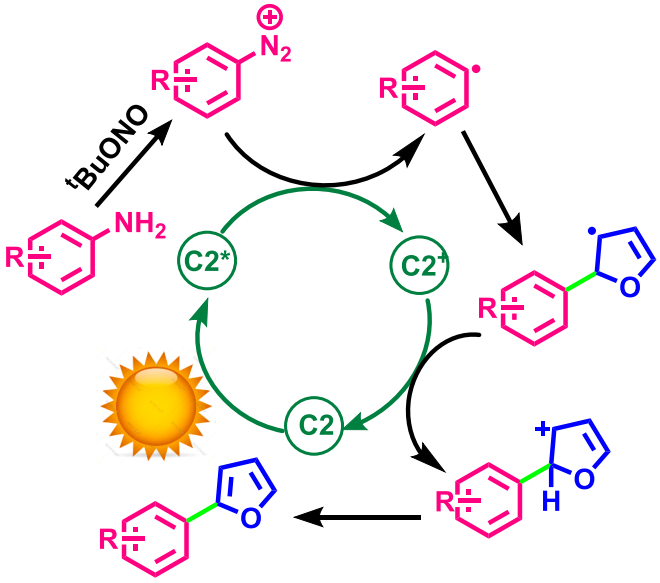

Fig. 4. Plausible mechanism of photoredox reaction.

measured λ_{max} values of the primary absorption bands of corroles (Table 11). As seen in Fig. 5, the HOMOs are localized on the corrole ring and three *meso*-aryl groups. In contrast, LUMOs are distributed on the corrole ring and the two *meso*-aryl rings (C-5, C-15 substituents). The calculated HOMO and LUMO gaps were similar for three corroles **C1-C3** and were in the range of 2.46 eV to 2.59 eV (Fig. 5).

The Electron Density Difference (EDD) plots help us to understand the charge distribution on the entire molecule. The computed electron density difference plots are shown in Fig. 6b and Figures S89-S90 of the SI. Analysis of electron density difference plots (Fig. 6b) between the first excited state and the ground state revealed yellow-colored lobes signifying electron-withdrawing regions and blue-colored lobes denoting electron-donating regions. The outer ends of the molecule exhibited yellow regions due to the presence of electron-withdrawing groups (EWG). The middle portion, featuring nitrogen atoms with lone pairs, displayed blue-colored lobes representing electron-donating groups (EDG). Corrole **C1** (Figure S89) exhibited a limited yellow color with only fluorine atoms as EWG. In contrast, Corrole **C2** and **C3** (Fig. 6b and Figure S90), incorporating resonance-stabilized EWG like –CN, displayed increased, yellow-colored lobes, emphasizing a more significant electron density increment for the cyanide group than fluorine.

Fig. 7 shows computed reaction energy profiles for C−H arylation of heteroarenes for corrole **C2**. All the energy calculations are done for the individual structures. The energy predictions derived from individual ground and excited state structures are inherently influenced by the number and type of substituents present on the molecule. These predictions serve as foundational elements in elucidating the mechanism and efficiency of the catalyst. By thoroughly analyzing the ground and excited state structures, we can gain valuable insights into the intricate interplay between the catalyst and reactants, thus facilitating a comprehensive understanding of catalyst performance. The additional reaction profiles for the three corrole systems have been incorporated into the Supplementary Information as Figures S91 and S92. Remarkably, all three systems exhibit similar energy profiles. In the initial step, the free energy differences (the difference between Gibbs free energies) for catalysts **C1** and **C2** are 7.63 and 3.44 kcal/mol, respectively. However, for the catalyst **C3**, this step represents a downhill process, with a corresponding Gibbs free energy difference of −0.38 kcal/mol. The subsequent step is consistent across all catalysts, characterized by a downhill progression with no energy requirement, indicated by a Gibbs free energy change of −24.73 kcal/mol. Following this, the third step, common to all catalysts, necessitates an uphill energy input of 7.30 kcal/mol. The fourth step exhibits very little differentiation among the catalysts, with energy requirements of approximately −44.76, −42.34, and −41.14 kcal/mol for each catalyst. Finally, the final step is again a downhill process shared among all catalysts, with a change in Gibbs free energy of −19.56 kcal/mol. This diagram explains the thermodynamics of the reaction.

In addition, the transition state calculations to estimate the barrier height (activation energies) for the reaction using different corroles were performed by using ORCA 5.0 software. We employed the method proposed by Yepes et al., utilizing the PBE functional with dispersion correction and the Def2-SVP basis set [59]. The pre-opt keyword was employed to reoptimize the reactants and products. To verify the transition state, we performed the frequency calculations, which validated the formation of the transition state. As shown in the Fig. 8, the activation energy barrier for the three catalysts is 49.7 kcal/mol (**C1**), 41.2 kcal/mol (**C2**), and 43.9 kcal/mol (**C3**). The normal mode imaginary frequencies of the corroles **C1**, **C2** and **C3** are −1373.7, −295.4 and −9.6 cm^{-1}, respectively. Although the difference among the catalysts is not huge, it agrees with the experimental results; as for **C2**, the least barrier exists, implying its better efficiency among the three corroles.

As the steps could be more distinguishable, we have calculated the redox potential values to distinguish the catalytic efficiency of the three systems (Table 12). We used the Latimer diagram to obtain the excited state redox potential values [60]. The computed redox potential values are tabulated in Table 12. The ground state redox potential values show that the corrole systems in the ground state cannot act as suitable donors and acceptors. However, as they get excited, the redox potential values become positive, showing the rings increasing tendency to donate and accept electrons. If we compare the electron-donating tendency or the oxidation potential of the excited state, corrole **C2** possesses slightly higher value, which means corrole **C2** can donate the electrons more spontaneously than corrole **C1** and **C3**. We considered the oxidation potential here because it directly affects the first step, which is the

Calcd. Mol. mass: **279.1703**
Observed Mol. mass: **279.1709**

Scheme 3. Entrapment of aryl radical by TEMPO to support radical mechanism.

Table 8
Optimization of solvent for borylation of heteroarenes.[a]

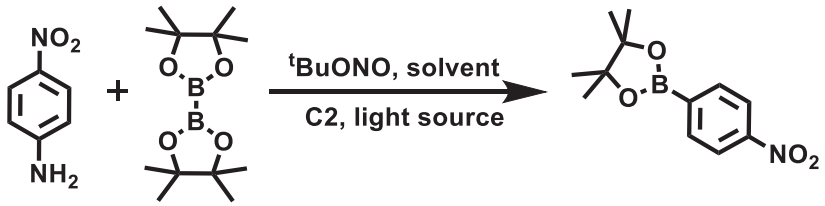

Entry	Solvent	Yield[b] (%)
1	DMSO	45 %
2	nitromethane	60 %
3	MeCN	71 %
4	DMF	51 %
5	MeOH	40 %
6	DCM	61 %
7	Toluene	35 %
8	$CHCl_3$	32 %

[a]Reaction conditions: 4-nitroaniline (0.23 mmol), bis(pinacolato)diboron (0.15 mmol), ^{t}BuONO (0.3 mmol), **C2** (1 mol%) irradiation with blue light (24 W) for 1h under N_2 atm at rt. [b] Isolated yields after purification.

Table 9
Scope of borylation of substituted anilines in blue light and sunlight.[a]

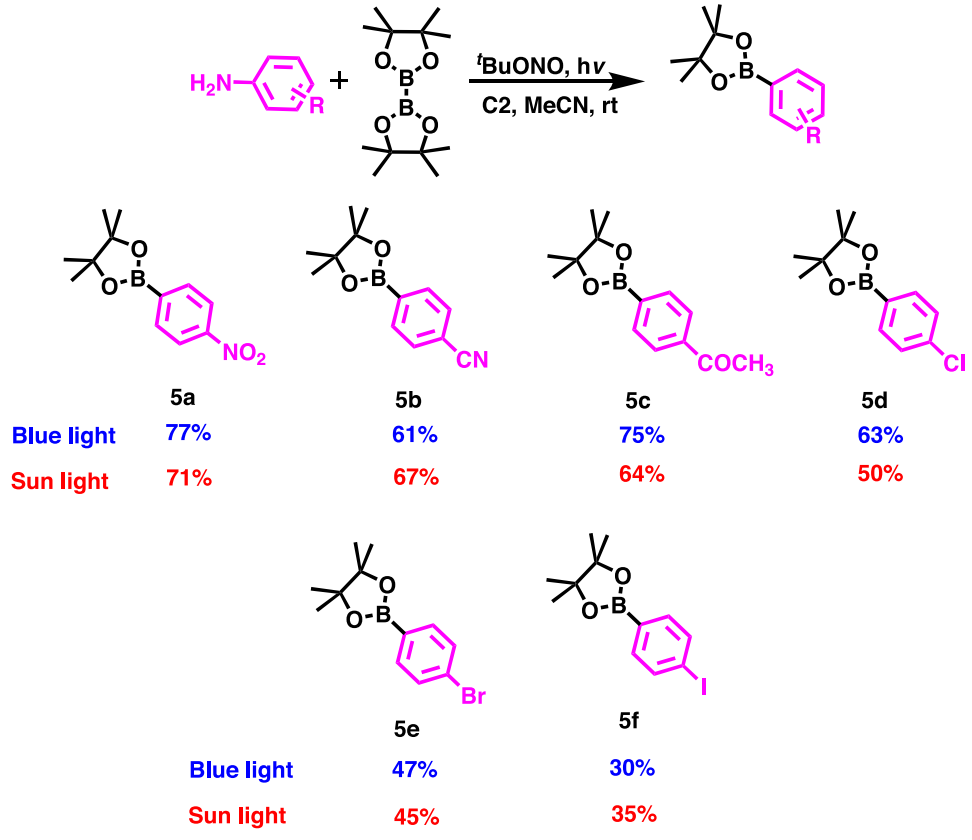

	5a	5b	5c	5d
Blue light	77%	61%	75%	63%
Sun light	71%	67%	64%	50%

	5e	5f
Blue light	47%	30%
Sun light	45%	35%

[a]Reaction conditions: Substituted anilines (0.23 mmol), bis(pinacolato)diboron (0.15 mmol), ^{t}BuONO (0.3 mmol) **C2** (1 mol%) irradiation with light (24 W) for 1h under N_2 atm at rt.

reactions distinguishable and rate-determining step. Moreover, the singlet state potential values are higher than the triplet state, which indicates that the reaction is likely to be more favourable via the singlet state.

For the radiative rate constant for the singlet state we have adopted a similar strategy as mentioned in literature [61]. From the rate constant values, it can be concluded that the emission is faster in the case of corrole **C1** and **C3** (higher value of rate constant in **C1** and **C3**), but for **C2** rate constant value is lower, so the lifetime of the **C2** excited state is more. The lifetime (inverse of fluorescence rate constant) is tabulated in Table 12. So, for **C2** there is more time available for the interaction of the ligand and the substrate due to which it should be more efficient in

Table 10
Scope of borylation of substituted anilines in blue light and sunlight.[a]

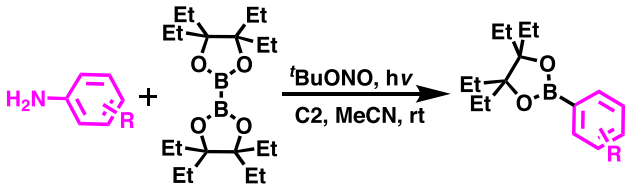

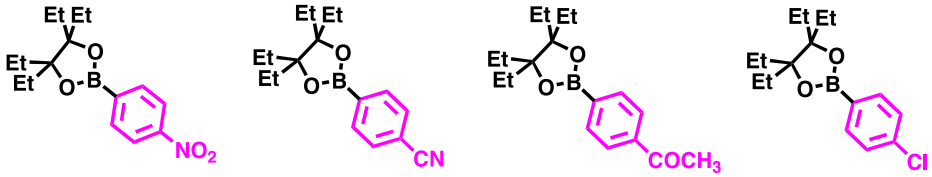

	6a	6b	6c	6d
Blue light	32%	26%	38%	34%
Sun light	20%	17%	23%	30%

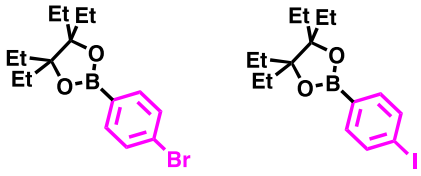

	6e	6f
Blue light	27%	15%
Sun light	30%	trace

[a]Reaction conditions: Substituted anilines (0.23 mmol), 4,4,4′,4′,5,5,5′,5′-Octaethyl-2,2′-bi-1,3,2-dioxaborolane (0.15 mmol), ^{t}BuONO (0.3 mmol), **C2** (1mol%), irradiation with light (24 W) for 1h under N_2 atm at rt.

comparison to that of **C1** and **C3**. Also, to study the charge transfer nature of the excited singlet state of the corroles, we have done the charge transfer calculations. Table 12 depicts the charge transfer numbers for each catalyst. Q_{CT} is the amount of charge perturbed when the molecule is excited from the ground to an excited state. Its value varies between 0 and 1 and is a unitless quantity. A Q_{CT} value near 1 signifies a charge transfer state, while a value near 0 results in a locally excited transition. To compute Q_{CT}, firstly, the two wavefunctions corresponding to the ground and excited states are generated with the help of ORCA and Multiwfn codes. The Q_{CT} number is calculated based on the density difference grid data — the quality of the grids varies from low to high. In this case, we have chosen quality as the medium.

Theoretically, the lower value of E_{ox}* may facilitate the organic reaction if a photocatalyst follows oxidative quenching pathway. However, in the previous study with porphyrin-based photocatalysts [30], the authors did not find a direct correlation between the E_{ox}* of the porphyrin photocatalysts and the % yields of the products. On comparing the data obtained by CV, fluorescence studies ($E_{0,0}$) and the excited state oxidation potentials E_{ox}* of three corrole catalysts, it was observed that **C2** has the most negative E_{ox}* value among the three catalysts (Table 3). Also, their singlet state lifetimes were comparable (Table 2), which makes it challenging to determine the catalytic efficiency of corroles. The nature of *meso*-aryl groups (EWG, EDG) on the corrole skeleton has profound effect on their electrochemical properties, which is associated with their catalytic efficiency for a particular reaction. This implies that all three catalysts show nearly the same efficacy, with **C2** performance is slightly better than the other two catalysts.

We performed the calculations with the CAM-B3LYP functional to include the long-range interactions. A thermodynamical picture of the reaction for the **C1** catalyst is provided in SI, Figure S96. As can be seen, the first and third steps of the reaction can be considered as the uphill steps (accompanied by the positive change in Gibbs free energy). The rest are downhill steps (accompanied by the negative change in Gibbs free energy). A similar reaction trend is also found in the case of B3LYP functional, as seen in Figure S91. Similarly, the emission wavelength of the **C1** catalyst at the B3LYP level of theory (641.9 nm) also exhibits close agreement with CAM-B3LYP functional (640.5 nm). The oxidation and reduction potential values for **C1** with the B3LYP method are 0.54 V and 1.38 V, while the CAM-B3LYP functional yielded are 0.56 and 1.55 V. The charge transfer (CT) number difference for **C1** between the two functional is only 0.062. CT number for CAM-B3LYP functional is 0.286, and with B3LYP functional, it is 0.224. In addition, we have provided the density difference plot of the **C1** catalyst with CAM-B3LYP functional as Figure S97 in SI for quantitative comparison.

4. Conclusion

In summary, A_3 and A_2B type corroles were synthesized and characterized by UV–vis, fluorescence, NMR and Mass spectroscopic techniques. Single crystal structure of A_2B corrole exhibited lower torsion angles between the *meso*-aryl group and the corrole ring plane, indicating better communication in the molecules. This reflected in the red shifted absorption bands and emission spectra of corroles. Corroles were screened for C–H arylation and borylation reactions with substituted anilines under blue light and sunlight. **C2** corrole having two pentafluorophenyl and one *meso-p*-cyanophenyl group worked slightly better

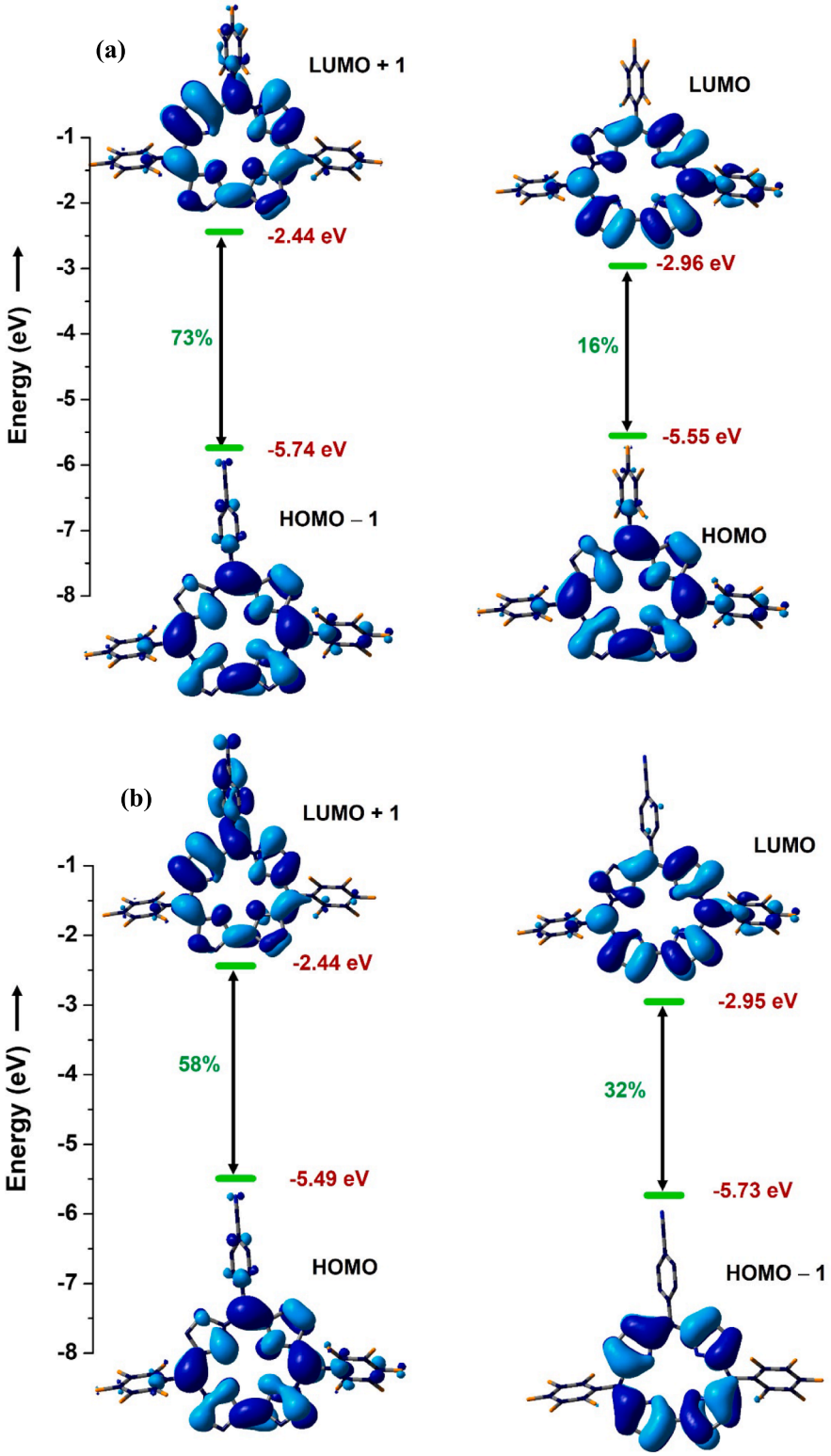

Fig. 5. Kohn–Sham orbital representations of frontier molecular orbitals and their corresponding energies of corroles (a) **C1,** (b) **C2** and (c) **C3**.

compared to **C1** and **C3** for photocatalytic transformations at room temperature. The method utilized 0.5 to 1 mol% of the corrole **C2** catalysts; it is versatile, non-toxic and efficient. Within 1–2 h of light exposure, the anilines with electron-donating and electron-withdrawing groups afforded moderate to good product yields. Corrole catalyst **C2** also worked efficiently in the sunlight, with comparable yields of the products as obtained under blue light irradiation. DFT studies supported the experimental findings in this work. The excited states redox potential data calculated by DFT indicated SET from the singlet state of **C2** catalyst to the diazonium salt generated *in-situ*. Overall, corrole based photo-redox catalysts are promising for C–H arylation reactions in the mild, green and energy efficient way.

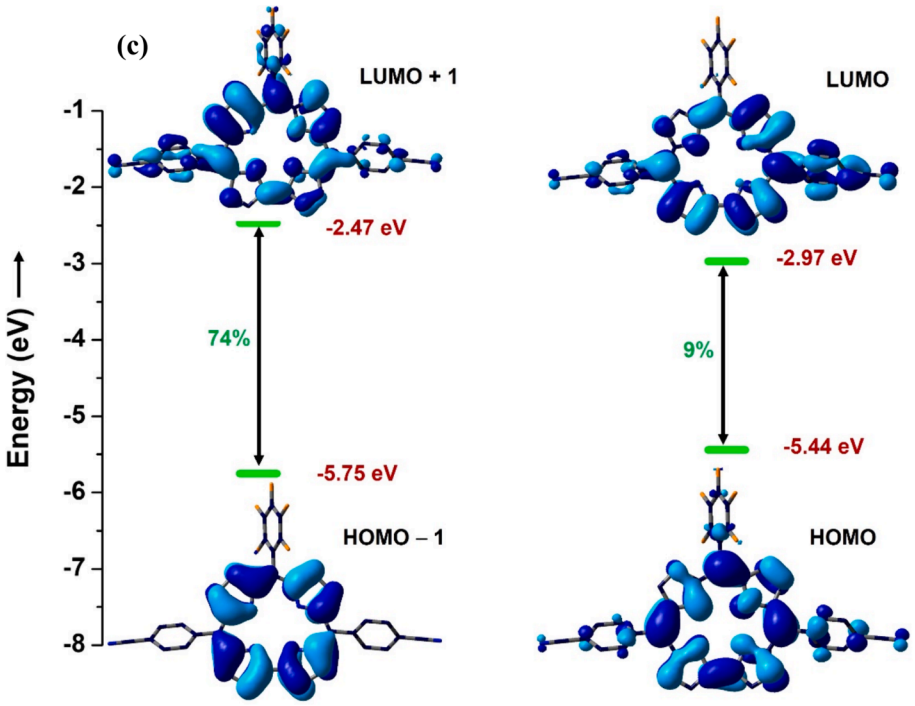

Fig. 5. (*continued*).

Table 11
Calculated excited state energies and their oscillatory strengths for corroles.

Corrole	Orbital Contribution (% coefficient)	Energy (eV)	Oscillatory strength (f)	Theoretical Absorption (nm)	Experimental Absorption (nm)
C1	HOMO-1 → LUMO+1 (73 %) HOMO→LUMO (16 %) HOMO→LUMO+1 (4 %)	2.59	1.33	394	414
C2	HOMO→LUMO+1 (58 %) HOMO-1 → LUMO (32 %) HOMO→LUMO+2 (7 %)	2.53	1.26	417	421
C3	HOMO-1 → LUMO+1 (74 %) HOMO→LUMO (9 %) HOMO→LUMO+2 (6 %) HOMO→LUMO+3 (7 %)	2.46	1.30	412	426

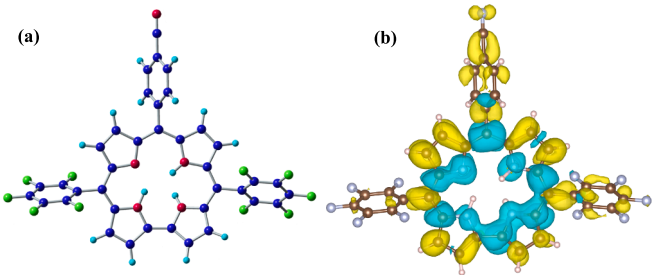

Fig. 6. (a) DFT optimized structure of corrole **C2**; (b) Electron Density Difference (EDD) plot for corrole **C2**.

5. General Experimental

5.1. General synthesis of corroles

The corroles catalysts **C1** and **C2** were prepared as described in the literature [62].

Synthesis of corrole C3.

In a 100 mL round bottom flask, 300 mg of 4-(di(*1H*-pyrrol-2-yl) methyl)benzonitrile (1.21 mmol, 1 equiv) and 75 µl of 2,3,4,5,6-pentafluorobenzaldehyde (0.607 mmol, 0.5 equiv) were taken and dissolved in pre-prepared solution of TFA in DCM (10 µl in 10 ml) and stirred in dark for 12 h. 446 mg of *p*-chloranil (1.81 mmol, 1.5 equiv) was added under oxygen atmosphere and was allowed to stir further for 5 h. After completion of reaction, reaction mixture was purified by neutral alumina column chromatography using 50 % DCM/hexane as an eluent.

5,10,15-Tris(pentafluorophenyl)corrole (C1) [63] Purple solid. ^{1}H NMR (500 MHz, Chloroform-*d*): δ (in ppm) 9.11 (d, *J*=4.0 Hz, 2H), 8.76 (d, *J*=5 Hz, 2H), 8.58 (d, *J*=4.5 Hz, 4H).

10-(4-Cyanophenyl)-5,15-bis(pentafluorophenyl)corrole (C2) [64] Purple solid. ^{1}H NMR (500 MHz, Chloroform-*d*): δ (in ppm) 9.14 (d, *J*=4.5 Hz, 2H), 8.74 (d, *J*=5.0 Hz, 2H), 8.61–8.59 (m, 4H), 8.31 (d, *J*=8.0 Hz, 2H), 8.07 (d, *J*=8.5 Hz, 2H).

10-(Pentafluorophenyl)-5,15-bis(4-Cyanophenyl)corrole (C3) Purple solid, mp > 225 °C. ^{1}H NMR (500 MHz, Chloroform-*d*): δ (in ppm) 9.03 (d, *J*=4.5 Hz, 2H), 8.88 (d, *J*=4.5 Hz, 2H), 8.57 (d, *J*=4.0 Hz, 2H), 8.51 (d, *J*=4.5 Hz, 2H), 8.46 (d, *J*=4.5 Hz, 4H), 8.12 (d, *J*=8.0 Hz, 4H). HRMS [ESI]: $C_{39}H_{20}F_5N_6^+$ $[M+H]^+$: calcd *m/z* 667.1664, found 667.1673.

General procedure for arylation of heteroarene.

In a 10 mL round bottom flask, substituted aniline (0.3 mmol, 1 equiv), heteroarene (3 mmol furan, 3 mmol thiophene or 0.6 mmol N-

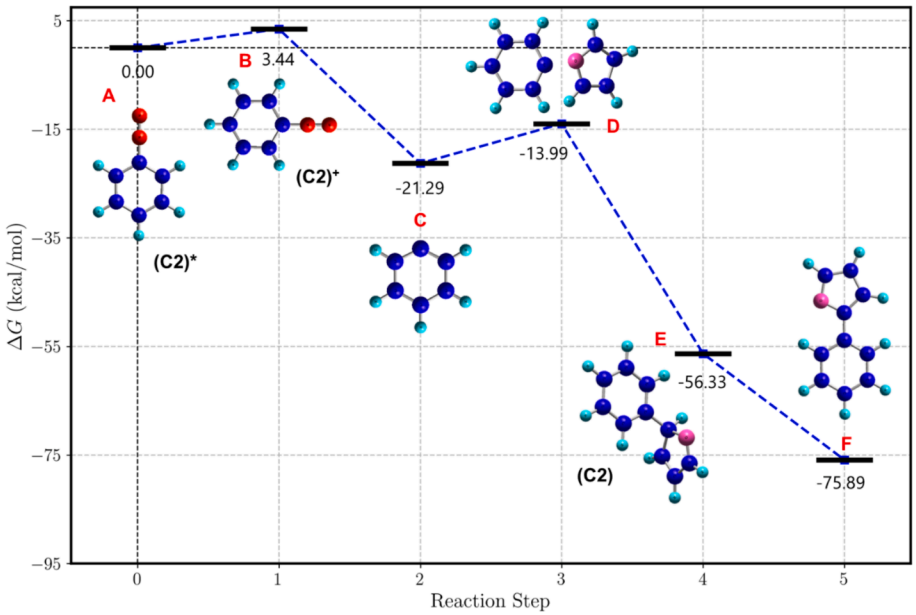

Fig. 7. Computed reaction profile for C−H arylation of heteroarenes. **(C2)** ground state of catalyst. **(C2)*** excited state of catalyst. **(C2)**$^{+}$ catalyst after SET.

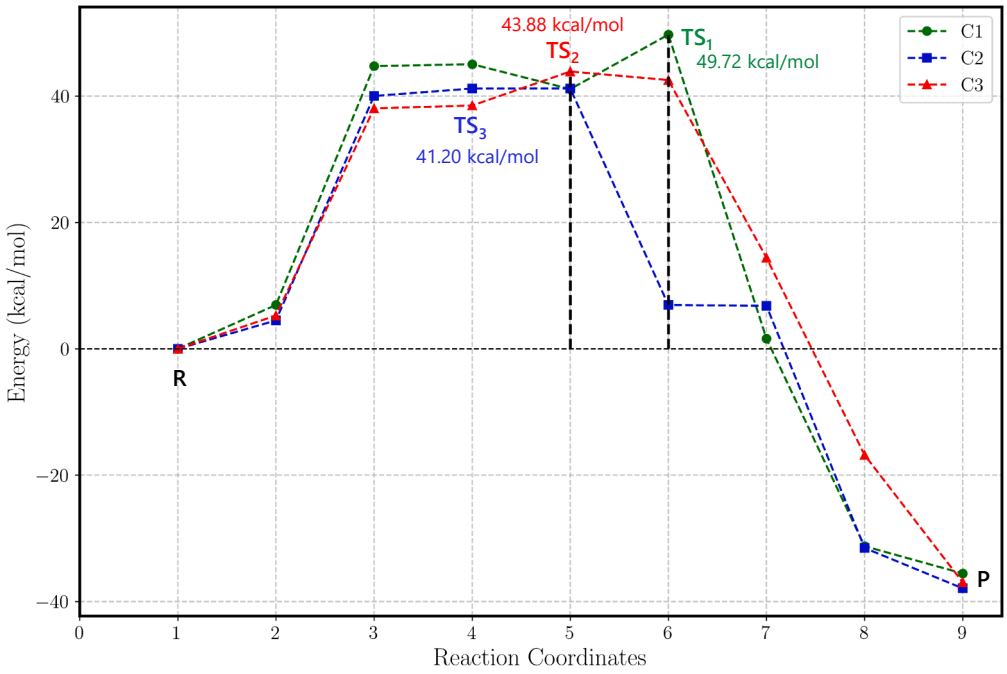

Fig. 8. Computed transition state profile diagram of C−H arylation of heteroarenes for all the three catalysts with dispersion corrected PBE functional [Marked point indicates reactant (R), product (P), transition state for Corrole **C1** (TS_1), **C2** (TS_2) and **C3** (TS_3). The remaining points depict intermediates.].

Table 12
Computed redox potential and fluorescence lifetime value of corroles. (ox-oxidation, red-reduction, ex-excited state).

	Corrole C1	Corrole C2	Corrole C3
E_{00}	1.94 eV	1.88 eV	1.73 eV
$E^{ox(gas)}$	−1.39 V	−1.29 V	−1.24 V
$E^{ox(ex)}$ (singlet)	0.54 V	0.59 V	0.50 V
$E^{ox(ex)}$ (triplet)	0.18 V	0.25 V	0.31 V
Fluorescence lifetime	7.7 ns	8.1 ns	6.2 ns
Q_{ct}	0.224	0.241	0.301

Boc pyrrole), and 1.1 mg of catalyst (0.5 mol%, 1.5×10^{-3} mmol) were weighed. 600 μL of DMSO was taken, followed by adding 0.45 mmol of *tert*-butyl nitrite. Reaction mixture was exposed to 440 nm blue light (Smartchem Synth Photoreactor, 24 W) and was allowed to stir for 30 min. The reaction was monitored by TLC every 15 min. The photoredox reaction was carried out using a similar procedure in the presence of sunlight for 30 min. The purification of the product was carried out by silica gel column chromatography using ethyl acetate/ hexane mixture and were confirmed by ^{1}H and ^{13}C NMR (Figure S5-S62).

2-(4-nitrophenyl)furan (2a).[65] Yellow solid, mp 145–147 °C, $\mathbf{R_f}$ = 0.3 (hexane:EtOAc, 10:1). ^{1}H NMR (500 MHz, Chloroform-*d*): δ (in ppm) 8.23 (d, *J*=9.0 Hz, 2H), 7.77 (d, *J*=9.0 Hz, 2H), 7.57 (s, 1H), 6.87

(d, *J*=3.5 Hz, 1H), 6.56–6.54 (m, 1H). ^{13}C{1H} NMR (125 MHz, Chloroform-*d*): δ (in ppm) 151.7, 146.4, 144.1, 136.4, 124.3, 123.9, 112.4, 108.9.

2-(2-bromo-4-chlorophenyl)furan (2b) [66]. Colourless viscous liquid, $\mathbf{R_f}$ = 0.7 (hexane). ^{1}H NMR (500 MHz, Chloroform-*d*): δ (in ppm) 7.72 (d, *J*=8.5 Hz, 1H), 7.65 (d, *J*=2.0 Hz, 1H), 7.51 (d, *J*=1.5 Hz, 1H), 7.34–7.32 (m, 1H), 7.17 (d, *J*=3.5 Hz, 1H), 6.53–6.52 (m, 1H). ^{13}C{1H} NMR (125 MHz, Chloroform-*d*): δ (in ppm) 150.3, 142.4, 133.6, 133.2, 129.8, 129.3, 127.7, 119.6, 111.5, 110.9.

4-(furan-2-yl)benzonitrile (2c) [67]. White solid, mp 76–78 °C, $\mathbf{R_f}$ = 0.2 (hexane:EtOAc, 10:1). ^{1}H NMR (500 MHz, Chloroform-*d*): δ (in ppm) 7.72 (d, *J*=8.5 Hz, 2H), 7.64 (d, *J*=8.0 Hz, 2H), 7.53 (s, 1H), 6.80 (d, *J*=3.5 Hz, 1H), 6.53–6.52 (m, 1H). ^{13}C{1H} NMR (125 MHz, Chloroform-*d*): δ (in ppm) 152.0, 143.7, 134.6, 132.6, 123.9, 118.9, 112.2, 110.3, 108.1.

1-(4-(furan-2-yl)phenyl)ethan-1-one (2d) [65]. White solid, mp 117–120 °C, $\mathbf{R_f}$ = 0.3 (hexane:EtOAc, 10:1). ^{1}H NMR (500 MHz, Chloroform-*d*): δ (in ppm) 7.97 (d, *J*=7.0 Hz, 2H), 7.73 (d, *J*=7.0 Hz, 2H), 7.53 (s, 1H), 6.80 (d, *J*=2.5 Hz, 1H), 6.52–6.51 (m, 1H), 2.61 (s, 3H). ^{13}C {1H} NMR (125 MHz, Chloroform-*d*): δ (in ppm) 197.4, 152.8, 143.3, 135.5, 134.9, 128.9, 123.5, 112.1, 107.4, 26.5.

2-(3,5-dichlorophenyl)furan (2e) [68]. Colourless solid, mp 72–74 °C $\mathbf{R_f}$ = 0.7 (hexane).^{1}H NMR (500 MHz, Chloroform-*d*): δ (in ppm) 7.52 (d, *J*=2.0 Hz, 2H), 7.48 (s, 1H), 7.22 (s, 1H), 6.95 (d, *J*=3.5 Hz, 1H), 6.49–6.48 (m, 1H). ^{13}C{1H} NMR (125 MHz, Chloroform-*d*): δ (in ppm) 151.2, 143.1, 135.3, 133.4, 126.9, 122.0, 111.9, 107.1.

2-(2,5-dichlorophenyl)furan (2f) [69]. Colourless viscous liquid, $\mathbf{R_f}$ = 0.7 (hexane). ^{1}H NMR (500 MHz, Chloroform-*d*): δ (in ppm) 7.86 (d, *J*=3.0 Hz, 1H), 7.52 (s, 1H), 7.24 (d, *J*=9.0 Hz, 1H), 7.18 (d, *J*=3.5 Hz, 1H), 7.18–7.14 (m, 1H), 6.54–6.53 (m, 1H). ^{13}C{1H} NMR (125 MHz, Chloroform-*d*): δ (in ppm) 148.9, 142.6, 132.9, 131.8, 130.4, 128.0, 127.7, 127.4, 111.9, 111.8.

2-(3,4-dichlorophenyl)furan (2g) [70]. Colourless viscous liquid, $\mathbf{R_f}$ = 0.6 (hexane). ^{1}H NMR (500 MHz, Chloroform-*d*): δ (in ppm) 7.74 (d, *J*=2.0 Hz, 1H), 7.48–7.47 (m, 2H), 7.42 (d, *J*=8.5 Hz, 1H), 6.67 (d, *J*=3.5 Hz, 1H), 6.49–6.48 (m, 1H). ^{13}C{1H} NMR (125 MHz, Chloroform-*d*): δ (in ppm) 151.6, 142.8, 132.9, 130.9, 130.7, 130.6, 125.5. 122.9, 111.9, 106.4.

2-(4-bromophenyl)furan (2h) [65]. White solid, mp 93–95 °C, $\mathbf{R_f}$ = 0.6 (hexane). ^{1}H NMR (500 MHz, Chloroform-*d*): δ (in ppm) 7.54–7.47 (m, 5H), 6.65 (d, *J*=3.5 Hz, 1H), 6.48–6.47 (m, 1H). ^{13}C{1H} NMR (125 MHz, Chloroform-*d*): δ (in ppm) 152.9, 142.4, 131.8, 129.8, 125.3, 121.0, 111.8, 105.5.

2-(4-iodophenyl)furan (2i) [71]. White solid, mp 112–114 °C, $\mathbf{R_f}$ = 0.6 (hexane). ^{1}H NMR (500 MHz, Chloroform-*d*): δ (in ppm) 7.69 (d, *J*=8.5 Hz, 2H), 7.47 (s, 1H), 7.39 (d, *J*=8.5 Hz, 2H), 6.66 (d, *J*=3.5 Hz, 1H), 6.48–6.47 (m, 1H). ^{13}C{1H} NMR (125 MHz, Chloroform-*d*): δ (in ppm) 153.0, 142.4, 137.7, 130.3, 125.4, 111.8, 105.6, 92.4.

2-(2-ethynylphenyl)furan (2j) [72]. Colourless viscous liquid, $\mathbf{R_f}$ = 0.6 (hexane). ^{1}H NMR (500 MHz, Chloroform-*d*): δ (in ppm) 7.83 (d, *J*=8.0 Hz, 1H), 7.56 (d, *J*=8.0 Hz, 1H), 7.49 (s, 1H), 7.41–7.38 (m, 2H), 7.22–7.19 (m, 1H), 6.51–6.50 (m, 1H), 3.40 (s, 1H). ^{13}C{1H} NMR (125 MHz, Chloroform-*d*): δ (in ppm) 151.6, 142.0, 134.6, 132.3, 129.1, 126.6, 125.5, 117.0, 111.6, 109.7, 83.6, 82.1.

2-(2-(phenylethynyl)phenyl)furan (2 k) [73]. Colourless viscous liquid, $\mathbf{R_f}$ = 0.4 (hexane). ^{1}H NMR (500 MHz, Chloroform-*d*): δ (in ppm) 7.88 (d, *J*=8.0 Hz, 1H), 7.61–7.49 (m, 4H), 7.40–7.35 (m, 5H), 7.24–7.22 (m, 1H), 6.52–6.51 (m, 1H). ^{13}C{1H} NMR (125 MHz, Chloroform-*d*): δ (in ppm) 152.1, 141.9, 133.7, 131.8, 131.5, 128.6, 128.5, 128.4, 126.7, 125.5, 123.3, 118.2, 111.7, 109.5, 103.1, 93.8, 89.5.

2-(2-(p-tolylethynyl)phenyl)furan (2 l). Yellow viscous liquid, $\mathbf{R_f}$ = 0.3 (hexane). ^{1}H NMR (500 MHz, Chloroform-*d*): δ (in ppm) 7.87 (d, *J*=8.0 Hz, 1H), 7.60–7.58 (d, *J*=8Hz, 1H), 7.50–7.35 (m, 5H), 7.24–7.17 (m, 3H), 6.53–6.52 (m, 1H), 2.38 (s, 3H). ^{13}C{1H} NMR (125 MHz, Chloroform-*d*): δ (in ppm) 152.1, 141.8, 138.6, 133.6, 131.7, 131.4, 129.2, 128.4, 126.7, 125.5, 120.3, 118.4, 111.7, 109.5, 94.0, 88.9, 21.5. HRMS [ESCi]: $C_{19}H_{14}O^+$ $[M]^+$: calcd *m/z* 258.1039, found 258.1052. ^{13}C{1H} NMR (125 MHz, Chloroform-*d*): δ (in ppm).

2-(4-nitrophenyl)thiophene (3a).[74] Yellow solid, mp 145–147 °C, $\mathbf{R_f}$ = 0.5 (hexane:EtOAc, 10:1). ^{1}H NMR (500 MHz, Chloroform-*d*): δ (in ppm) 8.23 (d, *J*=9.0 Hz, 2H), 7.74 (d, *J*=9.0 Hz, 2H), 7.48–7.44 (m, 2H), 7.16–7.14 (m, 1H). ^{13}C{1H} NMR (125 MHz, Chloroform-*d*): δ (in ppm) 146.6, 141.6, 140.6, 128.7, 127.6, 126.0, 125.7, 124.4.

2-(2-bromo-4-chlorophenyl)thiophene (3b).[75] Colourless viscous liquid, $\mathbf{R_f}$ = 0.6 (hexane). ^{1}H NMR (500 MHz, Chloroform-*d*): δ (in ppm) 7.69 (s, 1H), 7.41–7.39 (m, 2H), 7.32–7.31 (m, 2H), 7.11–7.09 (m, 1H). ^{13}C{1H} NMR (125 MHz, Chloroform-*d*): δ (in ppm) 140.5, 134.1, 133.9, 133.2, 132.5, 128.0, 127.6, 127.0, 126.4, 123.1.

4-(thiophen-2-yl)benzonitrile (3c).[76] White solid, mp 105–107 °C, $\mathbf{R_f}$ = 0.4 (hexane:EtOAc, 10:1). ^{1}H NMR (500 MHz, Chloroform-*d*): δ (in ppm) 7.69 (d, *J*=8.0 Hz, 2H), 7.64 (d, *J*=8.5 Hz, 2H), 7.43–7.40 (m, 2H), 7.14–7.12 (m, 1H). ^{13}C{1H} NMR (125 MHz, Chloroform-*d*): δ (in ppm) 142.0, 138.6, 132.7, 128.5, 127.0, 126.1, 125.1, 118.8, 110.5.

1-(4-(thiophen-2-yl)phenyl)ethan-1-one (3d).[77] White solid, mp 125–127 °C, $\mathbf{R_f}$ = 0.3 (hexane:EtOAc, 10:1). ^{1}H NMR (500 MHz, Chloroform-*d*): δ (in ppm) 7.96 (d, *J*=8.0 Hz, 2H), 7.72 (d, *J*=8.5 Hz, 2H), 7.52 (s, 1H), 6.79 (d, *J*=3.0 Hz, 1H), 6.51 (s, 1H), 2.60 (s, 3H). ^{13}C {1H} NMR (125 MHz, Chloroform-*d*): δ (in ppm) 197.3, 142.9, 138.8, 135.7, 129.1, 128.3, 126.4, 125.6, 124.6, 26.6.

2-(3,5-dichlorophenyl)thiophene (3e).[78] Colourless liquid, $\mathbf{R_f}$ = 0.7 (hexane). ^{1}H NMR (500 MHz, Chloroform-*d*): δ (in ppm) 7.46 (s, 3H), 7.33 (d, *J*=5.0 Hz, 1H), 7.31 (d, *J*=4.0 Hz, 1H), 7.09–7.08 (m, 1H). ^{13}C{1H} NMR (125 MHz, Chloroform-*d*): δ (in ppm) 141.2, 137.2, 135.4, 128.2, 127.1, 126.3, 124.6, 124.2.

2-(2,5-dichlorophenyl)thiophene (3f).[77] Colourless viscous liquid, $\mathbf{R_f}$ = 0.7 (hexane). ^{1}H NMR (500 MHz, Chloroform-*d*): δ (in ppm) 7.52 (s, 1H), 7.43–7.37 (m, 3H), 7.22–7.20 (m, 1H), 7.12–7.10 (m, 1H). ^{13}C{1H} NMR (125 MHz, Chloroform-*d*): δ (in ppm) 138.7, 134.6, 132.6, 131.5, 131.0, 128.4, 128.2, 127.2, 126.2.

2-(3,4-dichlorophenyl)thiophene (3 g).[72] Off-white solid, mp 62–64 °C, $\mathbf{R_f}$ = 0.6 (hexane). ^{1}H NMR (500 MHz, Chloroform-*d*): δ (in ppm) 7.68 (d, *J*=1.5 Hz, 1H), 7.42 (s, 2H), 7.32–7.31 (m, 1H), 7.30–7.29 (m, 1H), 7.09–7.07 (m, 1H). ^{13}C{1H} NMR (125 MHz, Chloroform-*d*): δ (in ppm) 141.6, 134.4, 132.9, 131.2, 130.7, 128.2, 127.5, 125.9, 125.0, 124.1.

2-(4-bromophenyl)thiophene (3 h).[79] Colourless viscous liquid, $\mathbf{R_f}$ = 0.6 (hexane). ^{1}H NMR (500 MHz, Chloroform-*d*): δ (in ppm) 7.50–7.46 (m, 4H), 7.29 (d, *J*=4.0 Hz, 2H), 7.08–7.07 (m, 1H). ^{13}C{1H} NMR (125 MHz, Chloroform-*d*): δ (in ppm) 143.1, 133.3, 131.9, 128.1, 127.4, 125.2, 123.5, 121.2.

2-(4-iodophenyl)thiophene (3i).[79] Colourless viscous liquid, $\mathbf{R_f}$ = 0.6 (hexane). ^{1}H NMR (500 MHz, Chloroform-*d*): δ (in ppm) 7.68 (d, *J*=8.5 Hz, 2H), 7.33 (d, *J*=8.5 Hz, 2H), 7.30–7.29 (m, 2H), 7.08–7.06 (m, 1H). ^{13}C{1H} NMR (125 MHz, Chloroform-*d*): δ (in ppm) 143.1, 137.9, 133.9, 128.1, 127.6, 125.3, 123.5, 92.6.

2-(2-ethynylphenyl)thiophene (3j)[72] Colourless viscous liquid, $\mathbf{R_f}$ = 0.6 (hexane). ^{1}H NMR (500 MHz, Chloroform-*d*): δ (in ppm) 7.63–7.59 (m, 2H), 7.54–7.52 (m, 1H), 7.38–7.34 (m, 2H), 7.27–7.23 (m, 1H), 7.11–7.09 (m, 1H), 3.25 (s, 1H). ^{13}C{1H} NMR (125 MHz, Chloroform-*d*): δ (in ppm) 141.7, 136.5, 129.2, 129.1, 127.3, 127.1, 127.0, 125.8, 119.6, 83.2, 81.6.

2-(2-(phenylethynyl)phenyl)thiophene (3 k).[80] Colourless viscous liquid, $\mathbf{R_f}$ = 0.3 (hexane). ^{1}H NMR (500 MHz, Chloroform-*d*): δ (in ppm) 7.64–7.58 (m, 3H), 7.51–7.49 (m, 2H), 7.37–7.32 (m, 5H), 7.28–7.24 (m, 1H), 7.13–7.11 (m, 1H). ^{13}C{1H} NMR (125 MHz, Chloroform-*d*): δ (in ppm) 142.2, 135.9, 133.7, 131.4, 129.0, 128.6, 128.4, 127.2, 127.1, 126.8, 125.9, 123.4, 120.6, 93.7, 89.5.

2-(2-(p-tolylethynyl)phenyl)thiophene (3 l). Colourless liquid, $\mathbf{R_f}$ = 0.2 (hexane). ^{1}H NMR (500 MHz, Chloroform-*d*): δ (in ppm)

7.68–7.61 (m, 3H), 7.42 (d, *J*=8Hz, 2H), 7.40–7.34 (m, 2H), 7.30–7.28 (m, 1H), 7.18–7.14 (m, 3H), 2.39 (s, 3H). ^{13}C{1H} NMR (125 MHz, Chloroform-*d*): δ (in ppm) 142.2, 138.4, 135.8, 133.5, 131.3, 129.1, 128.8, 128.4, 127.1, 127.0, 126.7, 125.7, 120.7, 120.3, 93.9, 88.8, 21.5. HRMS [ESI]: $C_{19}H_{15}S^+$ $[M+H]^+$: calcd *m/z* 275.0889, found 275.0871. ^{13}C{1H} NMR (125 MHz, Chloroform-*d*): δ (in ppm).

***tert*-butyl 2-(4-nitrophenyl)-1H-pyrrole-1-carboxylate (4a).**[81] Yellow solid, mp 134–136 °C, $\mathbf{R_f}$ = 0.4 (hexane:EtOAc, 9:1). ^{1}H NMR (500 MHz, Chloroform-*d*): δ (in ppm) 8.21 (d, *J*=8.5 Hz, 2H), 7.50 (d, *J*=9 Hz, 2H), 7.41–7.40 (m, 1H), 6.33–6.32 (m, 1H), 6.28–6.26 (t, *J*=3.5, 1H), 1.43 (s, 9H). ^{13}C{1H} NMR (125 MHz, Chloroform-*d*): δ (in ppm) 148.9, 146.6, 140.7, 132.7, 129.5, 124.3, 122.9, 116.2, 111.1, 84.5, 27.7.

***tert*-butyl 2-(4-cyanophenyl)-1H-pyrrole-1-carboxylate (4b).**[82] Colourless viscous liquid, $\mathbf{R_f}$ = 0.4 (hexane:EtOAc, 9:1). ^{1}H NMR (500 MHz, Chloroform-*d*): δ (in ppm) 7.62 (d, *J*=8.5 Hz, 2H), 7.44 (d, *J*=8.0 Hz, 2H), 7.39–7.38 (m, 1H), 6.27–6.25 (m, 2H), 1.41 (s, 9H). ^{13}C {1H} NMR (125 MHz, Chloroform-*d*): δ (in ppm) 148.9, 146.6, 140.7, 132.7, 129.5, 124.3, 122.9, 116.5, 111.1, 84.5, 27.7.

***tert*-butyl 2-(4-acetylphenyl)-1H-pyrrole-1-carboxylate (4c).**[83] Colourless viscous liquid, $\mathbf{R_f}$ = 0.3 (hexane:EtOAc, 9:1) ^{1}H NMR (500 MHz, Chloroform-*d*): δ (in ppm) 7.94 (d, *J*=8.5 Hz, 2H), 7.44 (d, *J*=8.5 Hz, 2H), 7.38–7.37 (m, 1H), 6.27–6.24 (m, 2H), 2.61 (s, 3H), 1.39 (s, 9H). ^{13}C{1H} NMR (125 MHz, Chloroform-*d*): δ (in ppm) 197.7, 149.1, 139.0, 135.5, 133.9, 129.0, 127.7, 123.6, 115.5, 110.9, 84.1, 27.6, 26.4.

***tert*-butyl 2-(4-iodophenyl)-1H-pyrrole-1-carboxylate (4d).**[84] Colourless viscous liquid, $\mathbf{R_f}$ = 0.6 (hexane:EtOAc, 9:1). ^{1}H NMR (500 MHz, Chloroform-*d*): δ (in ppm) 7.66 (d, *J*=8.5 Hz, 2H), 7.34 (s, 1H), 7.10–7.08 (m, 2H), 6.21 (s, 1H), 6.18 (s, 1H), 1.39 (s, 9H). ^{13}C{1H} NMR (125 MHz, Chloroform-*d*): δ (in ppm) 149.1, 136.6, 133.9, 133.8, 130.9, 122.9, 114.8, 110.7, 92.7, 83.9, 27.6.

5.2. General procedure for borylation of heteroarene

0.225 mmol or 1 equiv of substituted aniline and 0.15 mmol of bis (pinacolato)diborane/ 4,4,4′,4′,5,5,5′,5′-Octaethyl-2,2′-bi-1,3,2-dioxaborolane were dissolved in 1 mL acetonitrile (MeCN) taken in a 10 mL round bottom flask. 1.1 mg of **C2** catalyst (1 mol%, 1.5 × 10^{-3} mmol) and 0.3 mmol of *tert*-butyl nitrite was added. The reaction mixture was irradiated under the same light condition as heteroarylation and took 1–3 h to complete. The purification of the product was carried out by silica gel column chromatography using ethyl acetate/hexane mixture and were confirmed by ^{1}H NMR (Figure S63-S84).

4,4,5,5-tetramethyl-2-(4-nitrophenyl)-1,3,2-dioxaborolane (5a).[85] White solid, mp 109–110 °C, $\mathbf{R_f}$ = 0.3 (pentane:EA, 9:1). ^{1}H NMR (500 MHz, Chloroform-*d*): δ (in ppm) 8.18 (d, *J*=8.5 Hz, 2H), 7.95 (d, *J*=8.5 Hz, 2H), 1.36 (s, 12H).

4-(4,4,5,5-tetramethyl-1,3,2-dioxaborolan-2-yl)benzonitrile (5b).[85] White solid, mp 99–101 °C, $\mathbf{R_f}$ = 0.3 (pentane:EA, 9:1). ^{1}H NMR (500 MHz, Chloroform-*d*): δ (in ppm) 7.87 (d, *J*=8.0 Hz, 2H), 7.63 (d, *J*=8.5 Hz, 2H), 1.35 (s, 12H).

1-(4-(4,4,5,5-tetramethyl-1,3,2-dioxaborolan-2-yl)phenyl) ethan-1-one (5c).[85] White solid, mp 66–68 °C, $\mathbf{R_f}$ = 0.2 (pentane:EA, 9:1). ^{1}H NMR (500 MHz, Chloroform-*d*): δ (in ppm) 7.92 (d, *J*=8.0 Hz, 2H), 7.88 (d, *J*=8.0 Hz, 2H), 2.62 (s, 3H), 1.36 (s, 12H).

2-(4-chlorophenyl)-4,4,5,5-tetramethyl-1,3,2-dioxaborolane (5d).[86] White solid, mp 56–58 °C, $\mathbf{R_f}$ = 0.6 (pentane:EA, 20:1). ^{1}H NMR (500 MHz, Chloroform-*d*): δ (in ppm) 7.71 (d, *J*=8.5 Hz, 2H), 7.33 (d, *J*=8.5 Hz, 2H), 1.34 (s, 12H).

2-(4-bromophenyl)-4,4,5,5-tetramethyl-1,3,2-dioxaborolane (5e).[85] White solid, mp 68–70 °C, $\mathbf{R_f}$ = 0.6 (pentane:EA, 20:1). ^{1}H NMR (500 MHz, Chloroform-*d*): δ (in ppm) 7.64 (d, *J*=8.0 Hz, 2H), 7.49 (d, *J*=8.5 Hz, 2H), 1.33 (s, 12H).

2-(4-iodophenyl)-4,4,5,5-tetramethyl-1,3,2-dioxaborolane (5f).[85] White solid, mp 90–92 °C $\mathbf{R_f}$ = 0.6 (pentane:EA, 20:1). ^{1}H NMR (500 MHz, Chloroform-*d*): δ (in ppm) 7.71 (d, *J*=8.0 Hz, 2H), 7.50 (d, *J*=8.0 Hz, 2H), 1.33 (s, 12H).

4,4,5,5-tetraethyl-2-(4-nitrophenyl)-1,3,2-dioxaborolane (6a). Pale yellow liquid, $\mathbf{R_f}$ = 0.3 (pentane:EA, 9:1). ^{1}H NMR (500 MHz, Chloroform-*d*): δ (in ppm) 8.18 (d, *J*=9.0 Hz, 2H), 7.96 (d, *J*=8.5 Hz, 2H), 1.82–1.72 (m, 8H), 0.98–0.95 (t, *J*=7.5 Hz, 12H). ^{13}C{1H} NMR (125 MHz, Chloroform-*d*): δ (in ppm) 149.8, 135.6, 122.4, 89.6, 26.4, 8.8. HRMS [ESCi]: $C_{16}H_{24}BNO_4^+$ $[M]^+$: calcd *m/z* 305.1793, found 305.1801.

4-(4,4,5,5-tetraethyl-1,3,2-dioxaborolan-2-yl)benzonitrile (6b). Colourless viscous liquid, $\mathbf{R_f}$ = 0.3 (pentane:EA, 9:1). ^{1}H NMR (500 MHz, Chloroform-*d*): δ (in ppm) 7.89 (d, *J*=7.5 Hz, 2H), 7.63 (d, *J*=7.5 Hz, 2H), 1.82–1.72 (m, 8H), 0.97–0.94 (t, *J*=7.5 Hz, 12H). ^{13}C{1H} NMR (125 MHz, Chloroform-*d*): δ (in ppm) 135.1, 131.1, 118.9, 114.3, 89.5, 26.4, 8.8. HRMS [ESCi]: $C_{17}H_{25}BNO_2^+$ $[M+H]^+$: calcd *m/z* 286.1973, found 286.1993.

1-(4-(4,4,5,5-tetraethyl-1,3,2-dioxaborolan-2-yl)phenyl)ethan-1-one (6c).[87] Colourless viscous liquid, $\mathbf{R_f}$ = 0.3 (pentane:EA, 9:1). ^{1}H NMR (500 MHz, Chloroform-*d*): δ (in ppm) 7.92 (d, *J*=8.0 Hz, 2H), 7.89 (d, *J*=8.0 Hz, 2H), 2.61 (s, 3H), 1.82–1.62 (m, 8H), 0.98–0.95 (t, *J*=7.5 Hz, 12H). ^{13}C{1H} NMR (125 MHz, Chloroform-*d*): δ (in ppm) 198.5, 138.9, 134.9, 127.2, 89.2, 26.7, 26.4, 8.8.

2-(4-chlorophenyl)-4,4,5,5-tetraethyl-1,3,2-dioxaborolane (6d). Colourless viscous liquid, $\mathbf{R_f}$ = 0.5 (pentane:EA, 20:1). ^{1}H NMR (500 MHz, Chloroform-*d*): δ (in ppm) 7.73 (d, *J*=8.5 Hz, 2H), 7.32 (d, *J*=8.5 Hz, 2H), 1.80–1.69 (m, 8H), 0.97–0.94 (t, *J*=7.0 Hz, 12H). ^{13}C{1H} NMR (125 MHz, Chloroform-*d*): δ (in ppm) 137.3, 136.1, 127.9, 89.0, 26.4, 8.8. MS [ESCi]: $C_{16}H_{24}BClO_2Na^+$ $[M+Na]^+$: calcd *m/z* 317.145, found 317.217.

2-(4-bromophenyl)-4,4,5,5-tetraethyl-1,3,2-dioxaborolane (6e). Colourless viscous liquid, $\mathbf{R_f}$ = 0.5 (pentane:EA, 20:1). ^{1}H NMR (500 MHz, Chloroform-*d*): δ (in ppm) 7.66 (d, *J*=8.5 Hz, 2H), 7.49 (d, *J*=8.0 Hz, 2H), 1.80–1.69 (m, 8H), 0.97–0.94 (t, *J*=7.5 Hz, 12H). ^{13}C{1H} NMR (125 MHz, Chloroform-*d*): δ (in ppm) 136.3, 130.9, 126.0, 89.0, 26.4, 8.8. MS [ESCi]: $C_{16}H_{24}BBrO_2^+$ $[M]^+$: calcd *m/z* 338.104, found 338.373.

4,4,5,5-tetraethyl-2-(4-iodophenyl)-1,3,2-dioxaborolane (6f) [88]. Colourless viscous liquid, $\mathbf{R_f}$ = 0.5 (pentane:EA, 20:1). ^{1}H NMR (500 MHz, Chloroform-*d*): δ (in ppm) 7.70 (d, *J*=8.0 Hz, 2H), 7.51 (d, *J*=8.0 Hz, 2H), 1.78–1.70 (m, 8H), 0.96–0.93 (t, *J*=7.5 Hz, 12H). ^{13}C {1H} NMR (125 MHz, Chloroform-*d*): δ (in ppm) 136.8, 136.3, 98.6, 89.0, 26.4, 8.8.

CRediT authorship contribution statement

Ashmita Jain: Writing – original draft, Software, Methodology, Investigation, Data curation. **Shekhar Kumar:** Visualization, Validation, Methodology. **Sanyam: . Anirban Mondal:** Writing – review & editing, Software. **Iti Gupta:** Writing – review & editing, Supervision, Project administration, Funding acquisition, Conceptualization.

Declaration of competing interest

The authors declare that they have no known competing financial interests or personal relationships that could have appeared to influence the work reported in this paper.

Data availability

Data will be made available on request.

Acknowledgements

Financial support from IIT Gandhinagar and CSIR, Govt. of India (Grant No: 01/3132/23/EMR-II) is greatly acknowledged. AJ and SK thank IIT Gandhinagar for the fellowship and infrastructural support. Sanyam thanks CSIR for the fellowship. AM acknowledges the Param

Ananta for computational support.

Appendix A. Supplementary material

Supplementary data to this article can be found online at https://doi.org/10.1016/j.jcat.2024.115705.

References

[1] M. Majek, A.J. Wangelin, Acc. Chem. Res. 49 (2016) 2316–2327.
[2] S.P. Pitre, C.D. McTiernan, J.C. Scaiano, Acc. Chem. Res. 49 (2016) 1320–1330.
[3] R. Costa e Silva, L.O. da Silva, A. de Andrade Bartolomeu, T.J. Brocksom, K.T. de Oliveira, Beilstein J. Org. Chem. 16 (2020) 917–955.
[4] M.H. Shaw, J. Twilton, D.W.C. MacMillan, J. Org. Chem. 81 (2016) 6898–6926.
[5] C.S. Wang, P.H. Dixneuf, J.F. Soulé, Chem. Rev. 118 (2018) 7532–7585.
[6] K.R. Jasinska, W. Shan, K. Zawada, K.M. Kadish, D. Gryko, J. Am. Chem. Soc. 138 (2016) 15451–15458.
[7] S. Fukuzumi, Y.M. Lee, W. Nam, J. Porphyr. Phthalocyanines. 23 (2019) 2–12.
[8] V. Pandey, D. Jain, N. Pareek, I. Gupta, Inorganica Chim. Acta. 502 (2020) 119339.
[9] V. Pandey, A. Janaagal, A. Jain, S. Mori, I. Gupta, Dyes Pigm. 209 (2023) 110861.
[10] S.M.M. Lopes, M. Pineiro, T.M.V.D. Melo, Molecules 25 (2020) 3450.
[11] (a) X. Zhan, P. Yadav, Y. Diskin-Posner, N. Fridman, M. Sundararajan, Z. Ullah, Q. C. Chen, L.J.W. Shimon, A. Mahammed, D.G. Churchill, M.H. Baik, Z. Gross, Dalton Trans. 48 (2019) 12279–12286;
(b) A. Mahammed, K. Chen, J. Vestfrid, J. Zhao, Z. Gross, Chem. Sci. 10 (2019) 7091–7103.
[12] X. Zhan, S. Kolanu, S. Fite, Q.C. Chen, W. Lee, D.G. Churchill, Z. Gross, Photochem. Photobiol. Sci. 19 (2020) 996–1000.
[13] L.M. Reith, M. Stiftinger, U. Monkowius, G. Knör, W. Schoefberger, Inorg. Chem. 50 (2011) 6788–6797.
[14] C.M. Lemon, A.G. Maher, A.R. Mazzotti, D.C. Powers, M.I. Gonzalez, D.G. Nocera, Chem. Commun. 56 (2020) 5247–5250.
[15] Z. Gross, L. Simkhovich, N. Galili, Chem. Commun. 7 (1999) 599–600.
[16] J. Grodkowski, P. Neta, E. Fujita, A. Mahammed, L. Simkhovich, Z. Gross, J. Phys. Chem. a. 106 (2002) 4772–4778.
[17] I. Luobeznova, M. Raizman, I. Goldberg, Z. Gross, Inorg. Chem. 45 (2006) 386–394.
[18] G.E.M. Crisenza, P. Melchiorre, Nat. Commun. 11 (2020) 803.
[19] H. Takeda, O. Ishitani, Coord. Chem. Rev. 254 (2010) 346–354.
[20] M. Gratzel, Acc. Chem. Res. 14 (1981) 376–384.
[21] K. Kalyanasundaram, M. Grätzel, Coord. Chem. Rev. 77 (1998) 347–414.
[22] M. Rueping, S. Zhu, R.M. Koenigs, Chem. Commun. 47 (2011) 8679–8681.
[23] J.D. Nguyen, J.W. Tucker, M.D. Konieczynska, C.R.J. Stephenson, J. Am. Chem. Soc. 133 (2011) 4160–4163.
[24] M.A. Ischay, M.E. Anzovino, J. Du, T.P. Yoon, J. Am. Chem. Soc. 130 (2008) 12886–12887.
[25] G. Pandey, R. Laha, D. Singh, J. Org. Chem. 81 (2016) 7161–7171.
[26] E. Medina, B. Pinter, J. Phys. Chem. a. 124 (2020) 4223–4234.
[27] V. Srivastava, P.P. Singh, RSC Adv. 7 (2017) 31377–31392.
[28] M. Majek, F. Filace, A.J. Von Wangelin, Beilstein J. Org. Chem. 10 (2014) 981–989.
[29] D.P. Hari, P. Schroll, B. König, J. Am. Chem. Soc. 134 (2012) 2958–2961.
[30] K. Rybicka-Jasińska, B. König, D. Gryko, Eur. J. Org. Chem. 2017 (2017) 2104–2107.
[31] A. Janaagal, V. Pandey, S. Sabharwal, I. Gupta, J. Porphyr. Phthalocyanines. 25 (2021) 571–581.
[32] N. Balsukuri, S. Das, I. Gupta, New J. Chem. 39 (2015) 482–491.
[33] N. Manav, J. Chavda, S. Kidwai, R. Singh, S. Mori, I. Gupta, J. Porphyr. Phthalocyanines. 27 (2023) 1304–1312.
[34] N. Balsukuri, I. Gupta, Dyes Pigm. 144 (2017) 223–233.
[35] N. Manav, R. Singh, A. Janaagal, A.K.S. Yadav, V. Pandey, I. Gupta, New J. Chem. 46 (2022) 19310–19321.
[36] B.J. Littler, M.A. Miller, C.H. Hung, R.W. Wagner, D.F. O'shea, P.D. Boyle, J. S. Lindsey, J. Org. Chem. 64 (1999) 1391–1396.
[37] R. Paolesse, A. Marini, S. Nardis, A. Froiio, F. Mandoj, D.J. Nurco, L. Prodi, M. Montalti, K.M. Smith, J. Porphyr. Phthalocyanines. 7 (2003) 25–36.
[38] Z. Gross, N. Galili, L. Simkhovich, I. Saltsman, M. Botoshansky, D. Blăser, R. Boese, I. Goldberg, Org. Lett. 1 (1999) 599–602.
[39] A. Ghosh, T. Wondimagegn, A.B.J. Parusel, J. Am. Chem. Soc. 122 (2000) 5100–5104.
[40] T. Ding, E.A. Alemán, D.A. Modarelli, C.J. Ziegler, J. Phys. Chem. a. 109 (2005) 7411–7417.
[41] A. Mahammed, Z. Gross, J. Inorg. Biochem. 88 (2002) 305–309.
[42] A. Ghosh, K. Jynge, Chem. Eur. J. 3 (1997) 823–833.
[43] (a) J.R. Weinkauf, S.W. Cooper, A. Schweiger, C.C. Wamser, J. Phys. Chem. a. 107 (2003) 3486–3496;
(b) J.J. Weaver, K. Sorasaenee, M. Sheikh, R. Goldschmidt, E. Tkachenko, Z. Gross, H.B. Gray, J. Porphyr. Phthalocyanines. 8 (2004) 76–81.
[44] J. Shen, J. Shao, Z. Ou, W.E.B. Koszarna, D.T. Gryko, K.M. Kadish, Inorg. Chem. 45 (2006) 5.
[45] J.O. Trent, G.R. Clark, A. Kumar, W.D. Wilson, D.W. Boykin, J.E. Hall, R. R. Tidwell, B.L. Blagburn, S. Neidle, J. Med. Chem. 39 (1996) 4554–4562.
[46] H.N.C. Wong, Pure Appl. Chem. 68 (1996) 335–344.
[47] Y.I. Gorak, N.D. Obushak, V.S. Matiichuk, R.Z. Lytvyn, Russ. J. Org. Chem. 45 (2009) 541–550.
[48] S. Zhang, Z. Tang, W. Bao, J. Li, B. Guo, S. Huang, Y. Zhang, Y. Rao, Org. Biomol. Chem. 17 (2019) 4364–4369.
[49] D. Lai, S. Ghosh, A. Hajra, Org. Biomol. Chem. 19 (2021) 4397–4428.
[50] M. Wang, Z. Shi, Chem. Rev. 120 (2020) 7348–7398.
[51] J. Plescia, N. Moitessier, Eur. J. Med. Chem. 195 (2020) 112270.
[52] M. Jiang, H. Yang, H. Fu, Org. Lett. 18 (2016) 5248–5251.
[53] D. Hu, L. Wang, P. Li, Org. Lett. 19 (2017) 2770–2773.
[54] W. Zhang, Z. Zou, W. Zhao, S. Lu, Z. Wu, M. Huang, X. Wang, Y. Wang, Y. Liang, Y. Zhu, Y. Zheng, Y. Pan, Nat. Commun. 11 (2020) 2572.
[55] M.J. Frisch, G.W. Trucks, H.B. Schlegel, G.E. Scuseria, M.A. Robb, J.R. Cheeseman, G. Scalmani, V. Barone, B. Mennucci, G.A. Petersson, H. Nakatsuji, M. Caricato, X. Li, H.P. Hratchian, A.F. Izmaylov, J. Bloino, G. Zheng, J.L. Sonnenberg, M. Hada, M. Ehara, K. Toyota, R. Fukuda, J. Hasegawa, M. Ishida, T. Nakajima, Y. Honda, O. Kitao, H. Nakai, T. Vreven, J.A. Montgomery, J.E. Peralta, F. Ogliaro, M. Bearpark, J.J. Heyd, E. Brothers, K.N. Kudin, V.N. Staroverov, T. Keith, R. Kobayashi, J. Normand, K. Raghavachari, A. Rendell, J.C. Burant, S.S. Iyengar, J. Tomasi, M. Cossi, N. Rega, J.M. Millam, M. Klene, J.E. Knox, J.B. Cross, V. Bakken, C. Adamo, J. Jaramillo, R. Gomperts, R.E. Stratmann, O. Yazyev, A.J. Austin, R. Cammi, C. Pomelli, J.W. Ochterski, R.L. Martin, K. Morokuma, V.G. Zakrzewski, G.A. Voth, P. Salvador, J.J. Dannenberg, S. Dapprich, A.D. Daniels, O. Farkas, B.J. Foresman, J. V. Ortiz, J. Cioslowski, D.J. Fox, Gaussian 09 Revision A.02, Gaussian Inc., Wallingford, CT, 2009.
[56] F. Neese, Wiley Interdiscip. Rev. Comput. Mol. Sci. 2 (2012) 73–78.
[57] T. Lu, F. Chen, J. Comput. Chem. 33 (2012) 580–592.
[58] K. Momma, F. Izumi, J. Appl. Cryst. 44 (2011) 1272–1276.
[59] D. Yepes, F. Neese, B. List, G. Bistoni, J. Am. Chem. Soc. 142 (2020) 3613–3625.
[60] T.B. Demissie, K. Ruud, J.H. Hansen, Organometallics. 34 (2015) 4218–4228.
[61] (a) R. Sanyam, A.M. Khatua, J. Chem. Theory Comput. 19 (2023) 9290–9301;
(b) R. Sanyam, A.M. Khatua, J. Phys. Chem. a. 127 (2023) 10393–10405.
[62] D.T. Gryko, B. Koszarna, Org. Biomol. Chem. 1 (2003) 350–357.
[63] R. Paolesse, S. Nardis, F. Sagone, R.G. Khoury, J. Org. Chem. 66 (2001) 550–556.
[64] D.T. Gryko, K. Jadach, J. Org. Chem. 66 (2001) 4267–4275.
[65] C.Y. Zhou, P.W.H. Chan, C.M. Che, Org. Lett. 8 (2006) 325–328.
[66] A. Janaagal, A. Sanyam, I.G. Mondal, J. Org. Chem. 88 (2023) 9424–9431.
[67] S.E. Denmark, J.D. Baird, Org. Lett. 8 (2006) 793–795.
[68] Y.F. Liang, R. Steinbock, L. Yang, L. Ackermann, Angew. Chem. Int. Ed. 57 (2018) 10625–10629.
[69] L. Wang, J. Byun, R. Li, W. Huang, K.A.I. Zhang, Adv. Synth. Catal. 360 (2018) 4312–4318.
[70] A.S. Demir, O.M. Reis, M. Emrullahog, Tetrahedron. 58 (2002) 8055–8058.
[71] I.N. Houpis, D. Shilds, U. Nettekoven, A. Schnyder, E. Bappert, K. Weerts, M. Canters, W. Vermuelen, Org. Process. Res. Dev. 13 (2009) 598–606.
[72] K. Maeyama, N. Iwasawa, J. Org. Chem. 64 (1999) 1344–1346.
[73] T. Shibata, S. Takayasu, Heteroat. Chem. 25 (2014) 379–388.
[74] J.H. Li, Y. Liang, D.P. Wang, W.J. Liu, Y.X. Xie, D.L. Yin, J. Org. Chem. 70 (2005) 2832–2834.
[75] S. Gowrisankar, J. Seayad, Chem. Eur. J. 20 (2014) 12754–12758.
[76] C. Amatore, A. Jutand, S. Negri, J.F. Fauvarque, J. Organomet. Chem. 390 (1990) 389–398.
[77] G.P. Roth, V. Farina, L.S. Liebeskind, E.P. Cabrera, Tetrahedron. 36 (1995) 2191–2194.
[78] M.A. Ismail, H.M. El-Shafeai, R.K. Arafa, M.H. Abdel-Rhman, E. Abdel-Latif, W. M. El-Sayed, Chemistry Select. 6 (2021) 7644–7653.
[79] S. Hotta, H. Kimura, S.A. Lee, T. Tamaki, J. Heterocycl. Chem. 37 (2000) 281–286.
[80] V. Mamane, P. Hannen, A. Fürstner, Chem. Eur. J. 10 (2004) 4556–4575.
[81] L. Groenendaal, M.J. Bruining, E.H.J. Hendrickx, A. Persoons, J.A.J. Vekemans, E. E. Havinga, E.W. Meijer, Chem. Mater. 10 (1998) 226–234.
[82] G.A. Molander, B. Canturk, L.E. Kennedy, J. Org. Chem. 74 (2009) 973–980.
[83] S. Lou, G.C. Fu, Adv. Synth. Catal. 352 (2010) 2081–2084.
[84] D. Hata, M. Tobisu, T. Amaya, Bull. Chem. Soc. Jpn. 91 (2018) 1749–1751.
[85] T. Ishiyama, M. Murata, N. Miyaura, J. Org. Chem. 60 (1995) 7508–7510.
[86] M. Murata, S. Watanabe, Y. Masuda, J. Org. Chem. 62 (1997) 6458–6459.
[87] N. Oka, T. Yamada, H. Sajiki, S. Akai, T. Ikawa, Org. Lett. 24 (2022) 3510–3514.
[88] I. Takashi, O. Naoki, A. Shuji, Jpn. Pat. WO 2022/186098 A1, 2022.